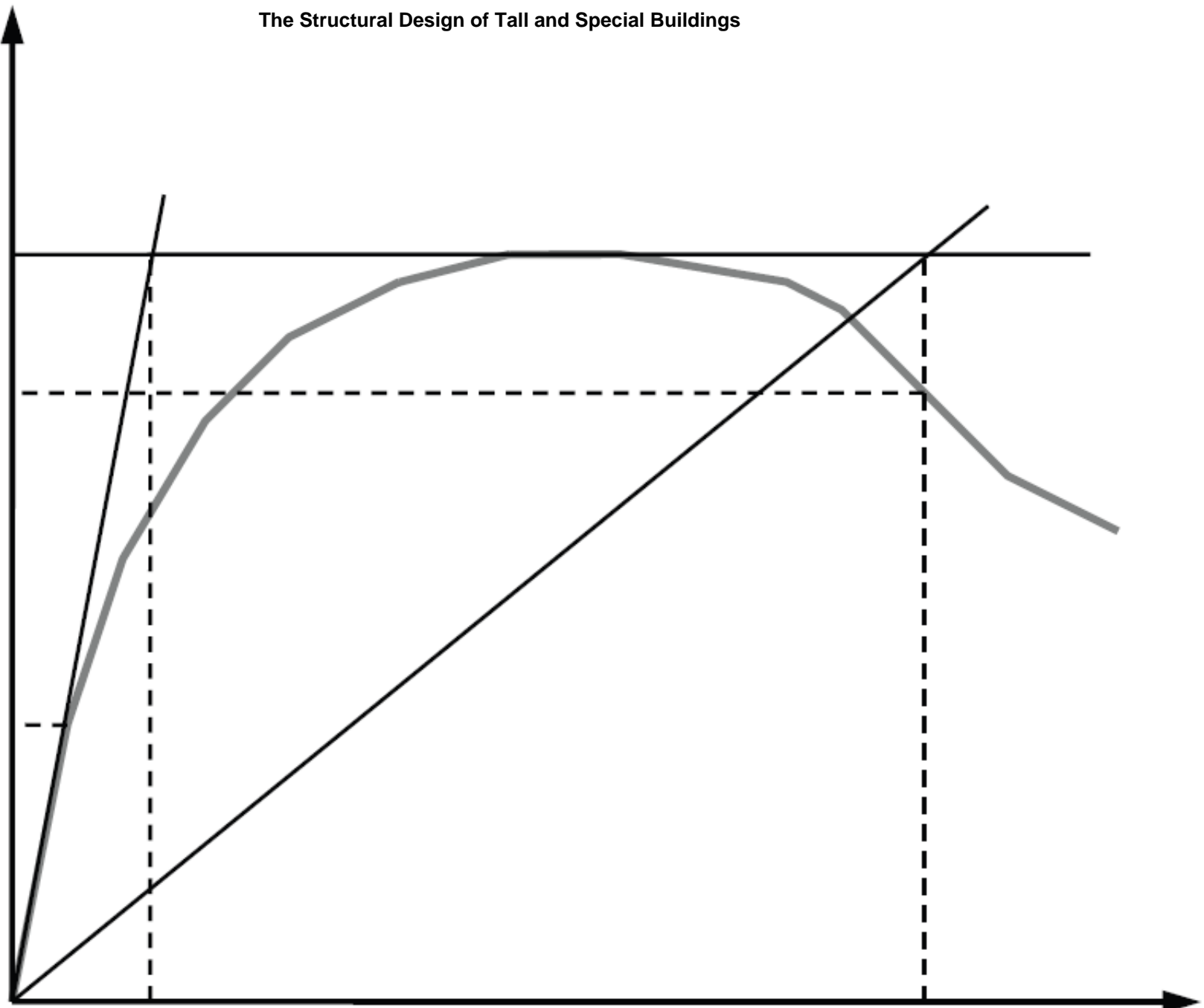


1
2
3
4
5
6
7
8
9
10
11
12
13
14
15
16
17
18
19
20
21
22
23
24
25
26
27
28
29
30
31
32
33
34
35
36
37
38
39
40
41
42
43
44
45
46
47
48

Base
Shear



V_{max}

$0.8V_{max}$

V

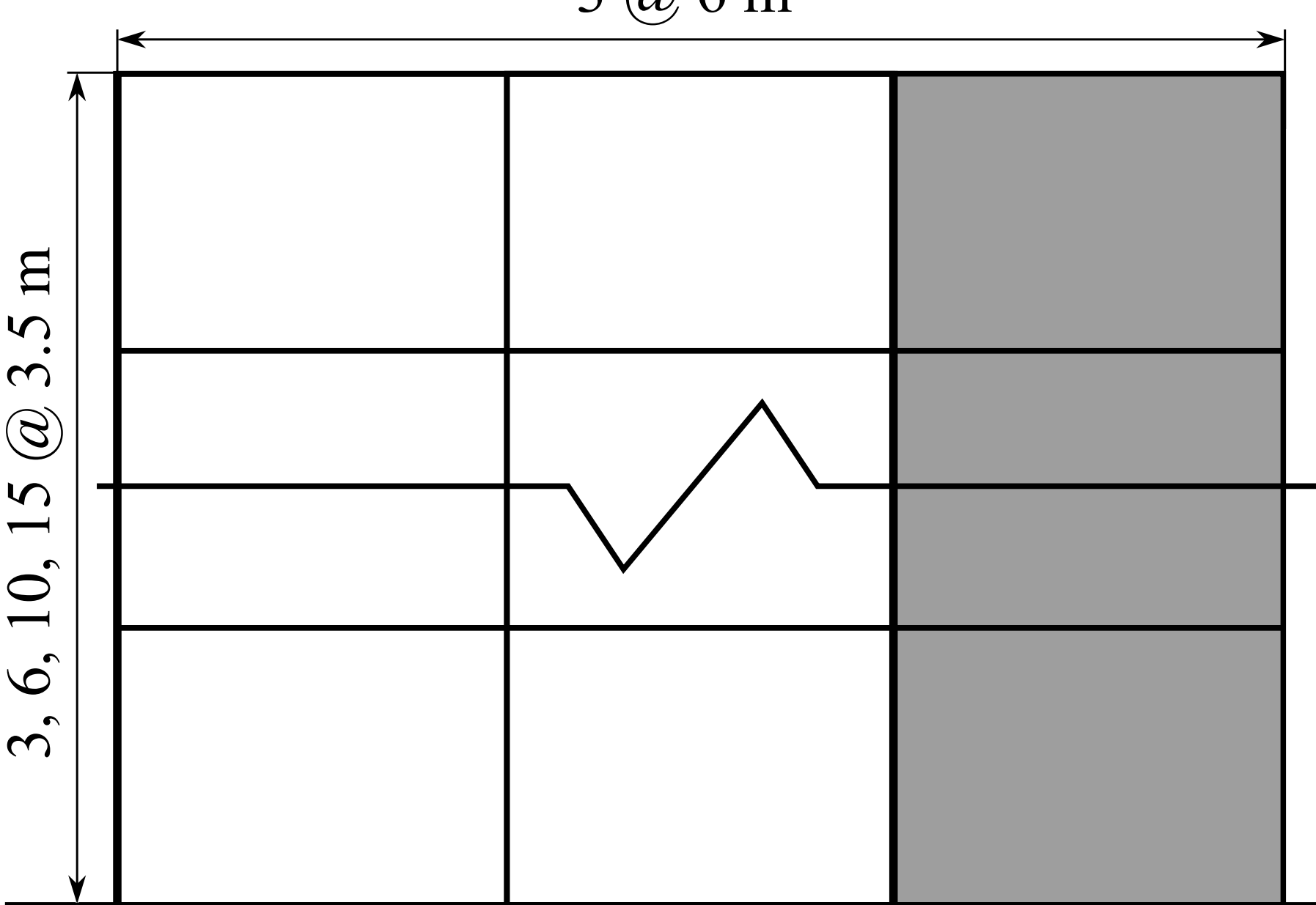
$\delta_{y,eff}$

δ_u

Roof Displacement

3 @ 6 m

3, 6, 10, 15 @ 3.5 m



Footing

1.0 m

19.6-20.0 m

Moment Frame

Flexure-Shear Interaction

Displacement-Based
Beam-Column Element

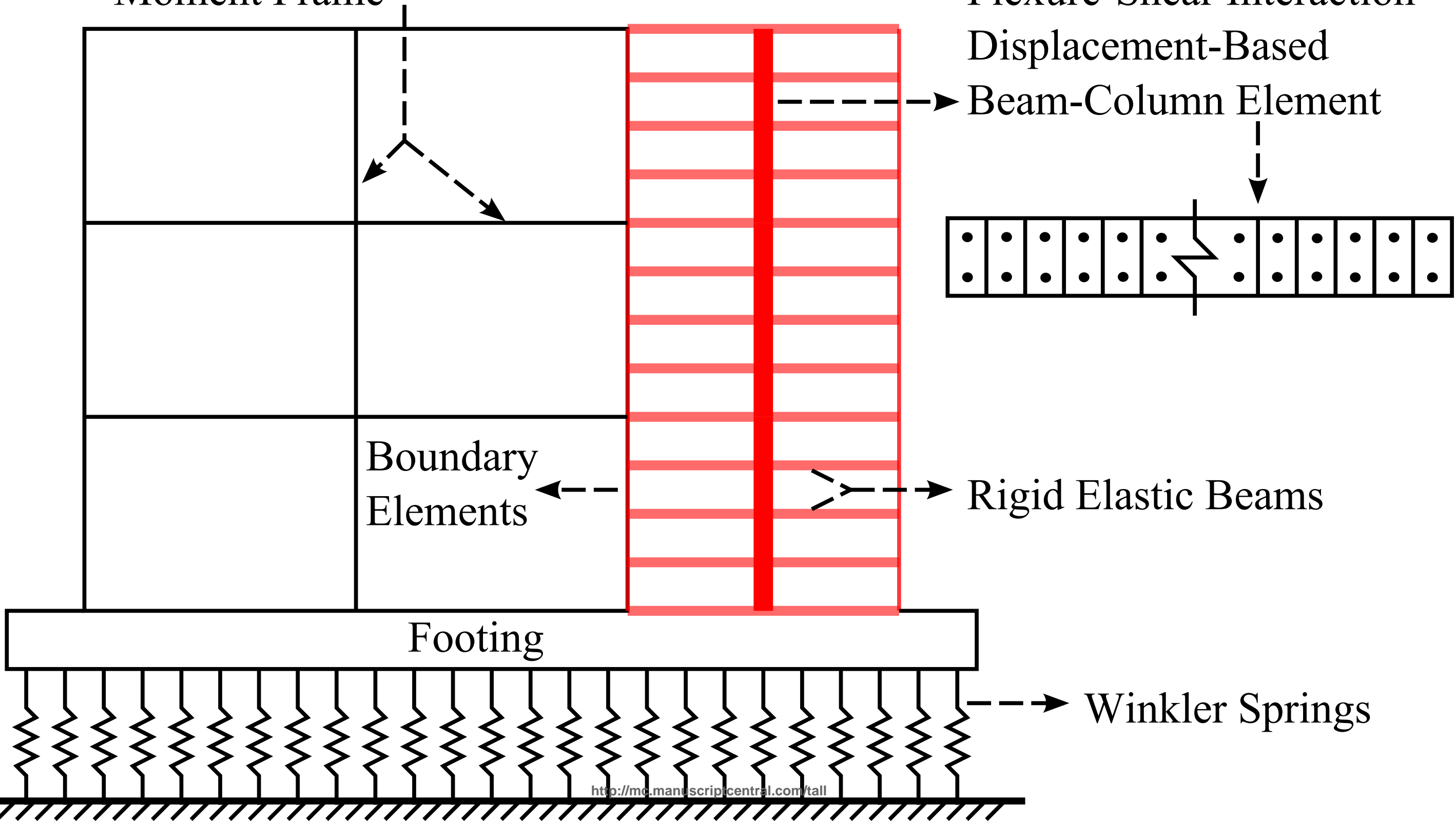
Boundary
Elements

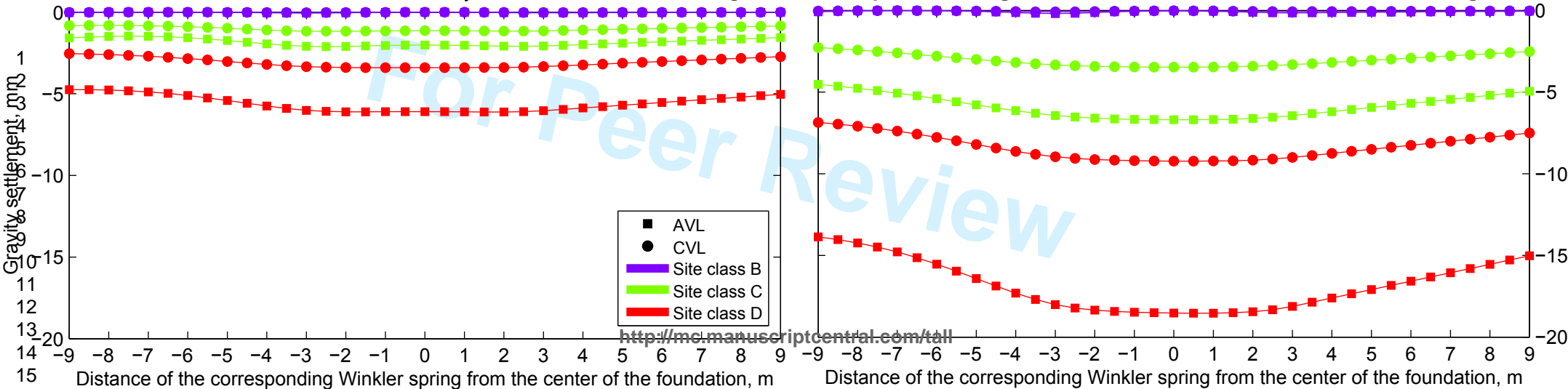
Rigid Elastic Beams

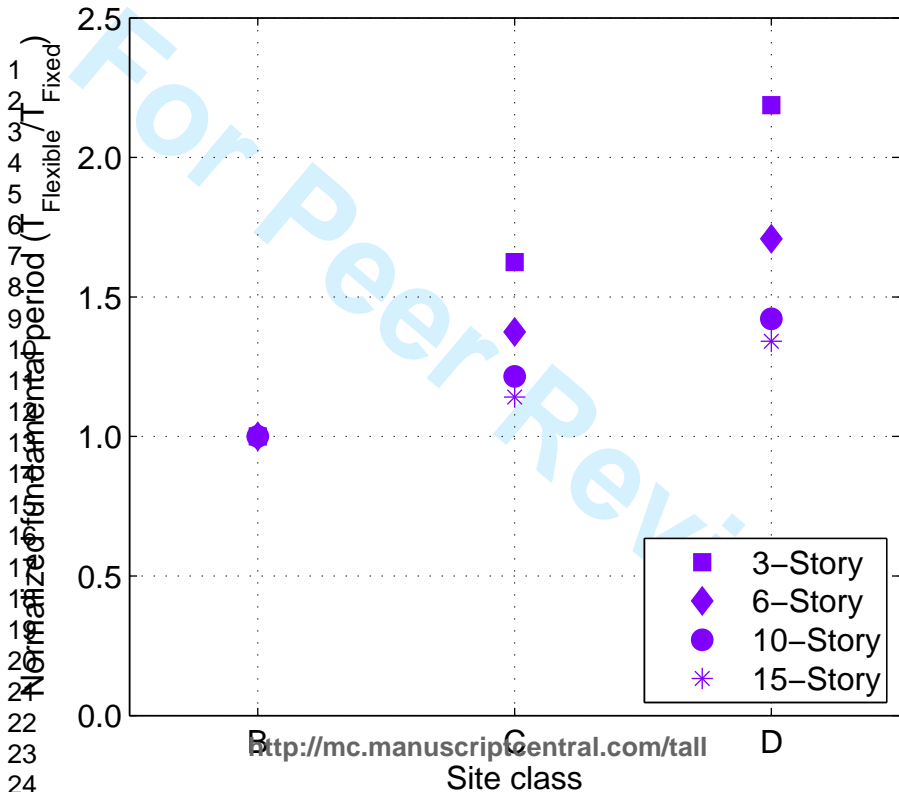
Footing

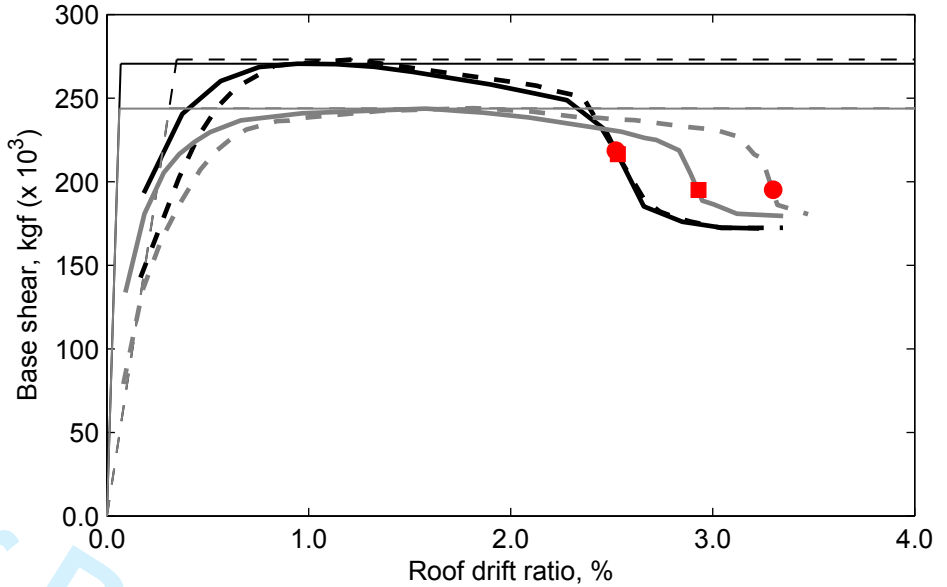
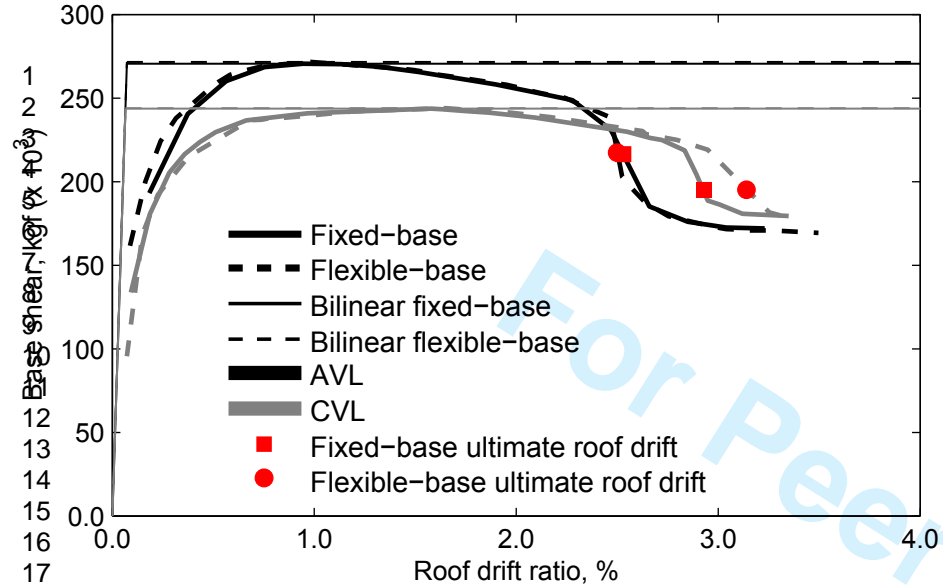
Winkler Springs

1
2
3
4
5
6
7
8
9
10
11
12
13
14
15
16
17
18
19
20
21
22
23
24
25
26
27
28
29
30
31
32
33
34
35
36
37
38
39
40
41
42
43
44
45
46
47
48
49
50
51
52

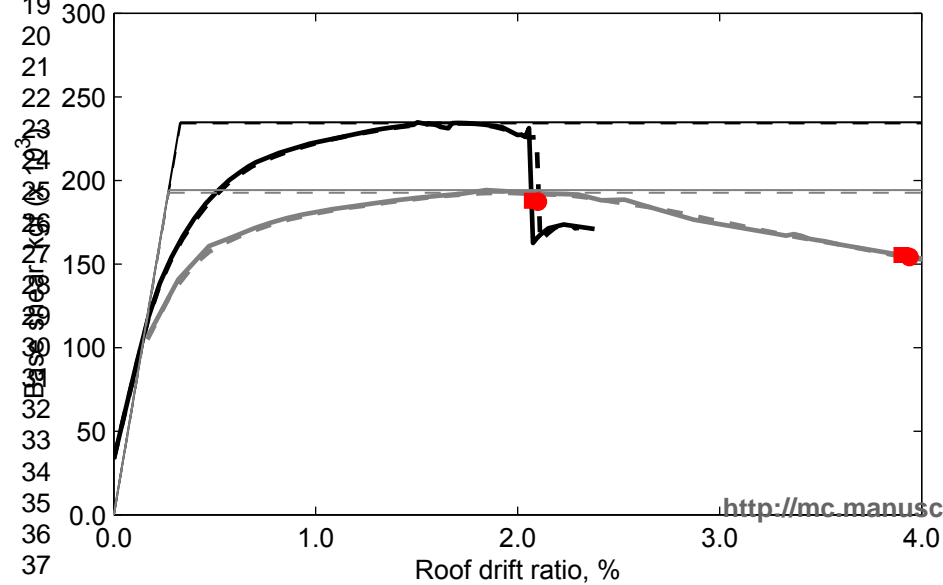




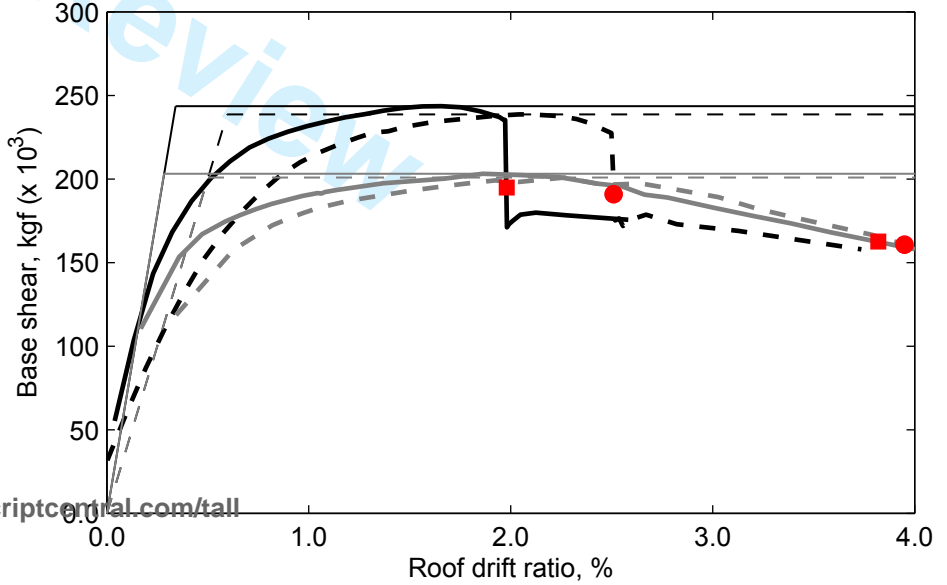




15-Story frames: Site class B

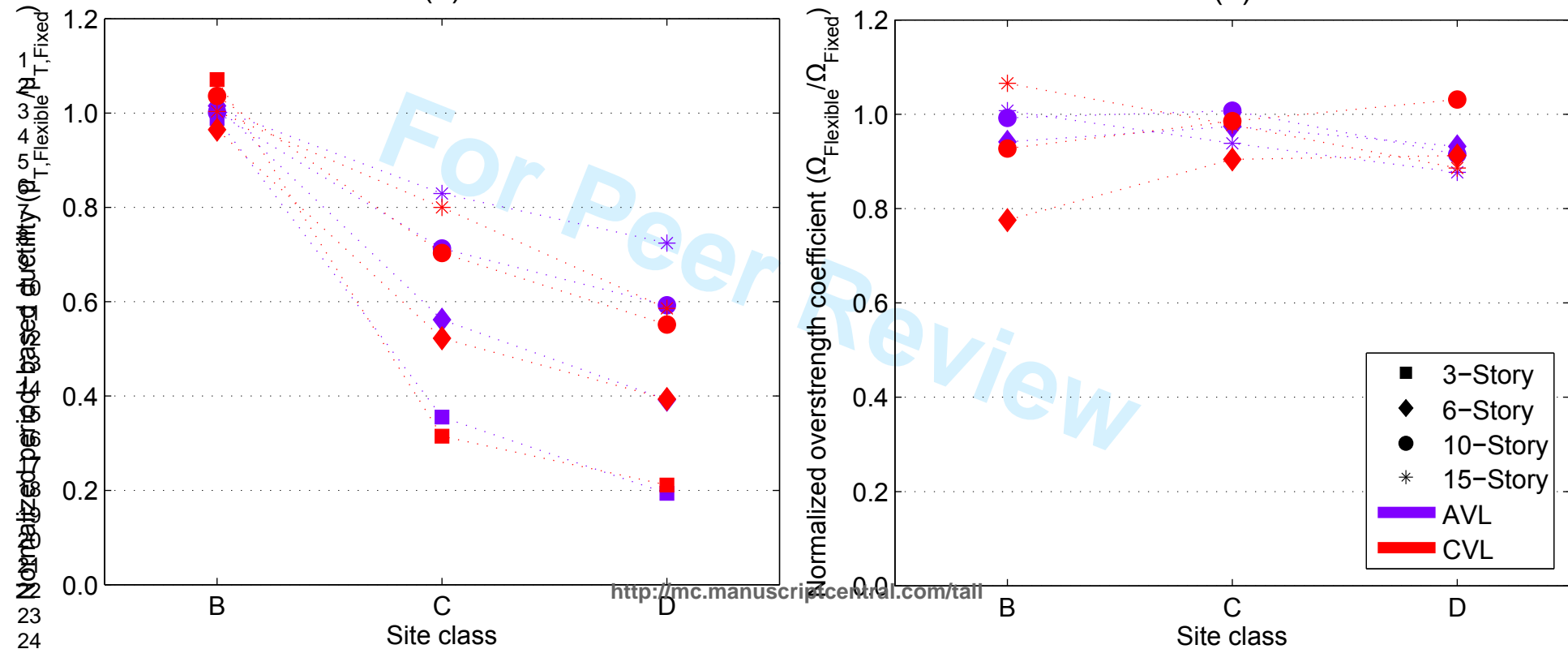


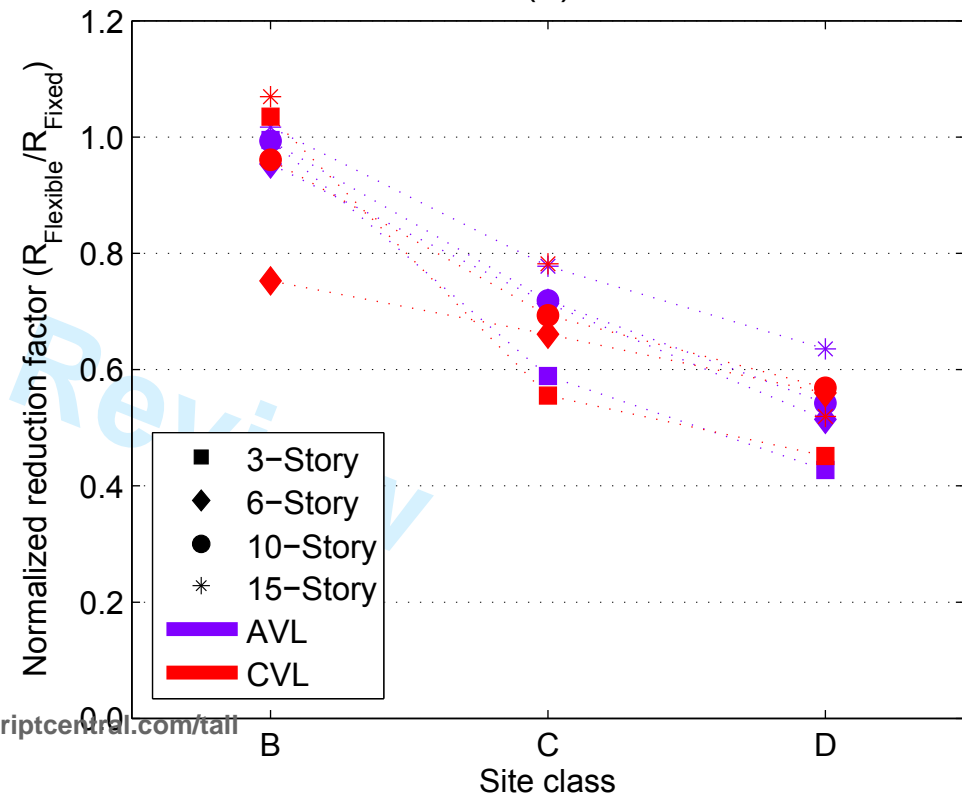
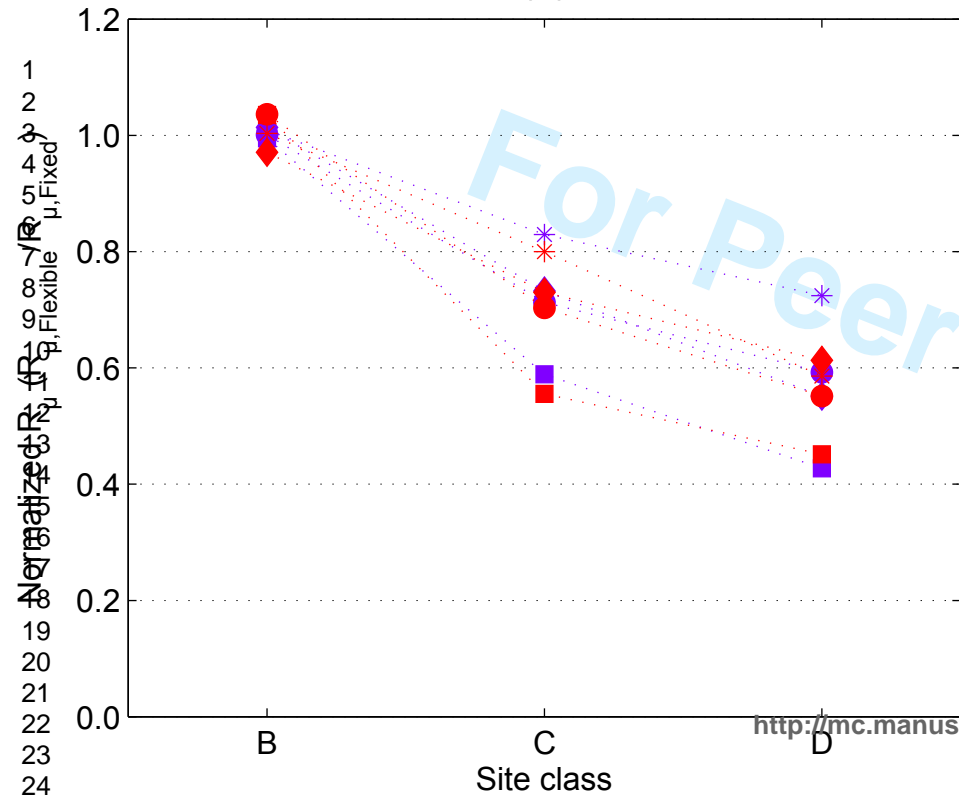
15-Story frames: Site class D



(a) The Structural Design of Tall and Special Buildings

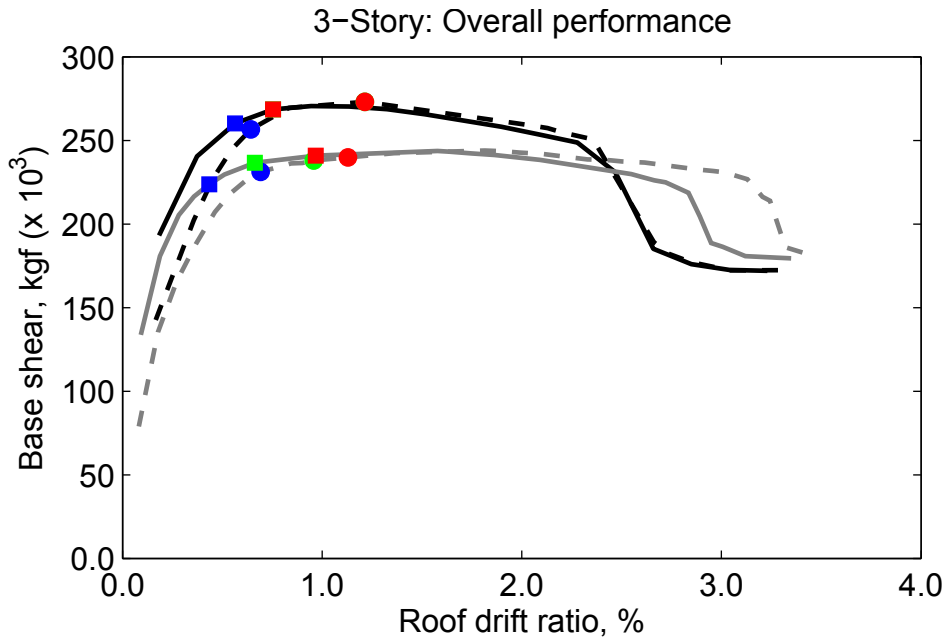
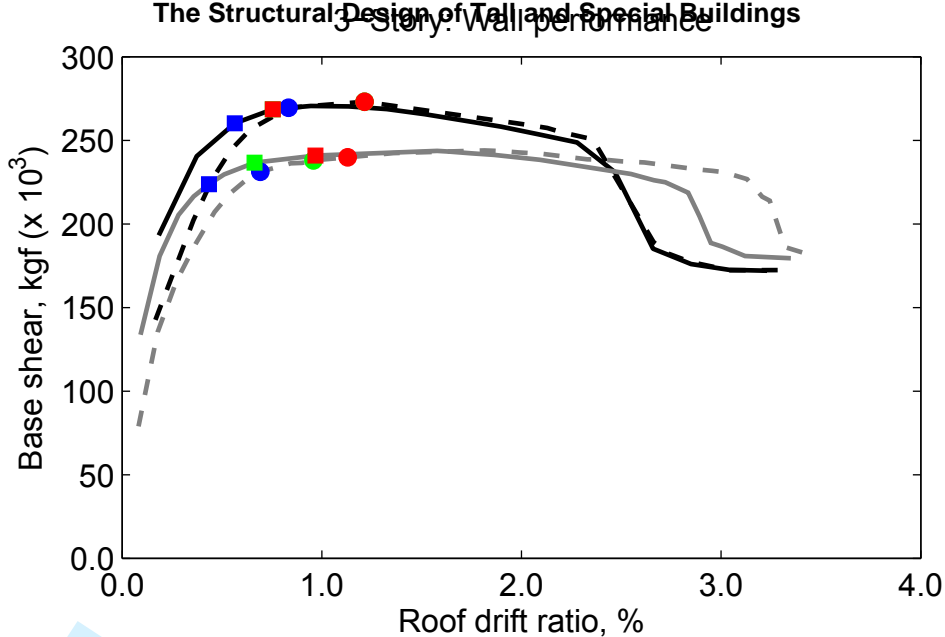
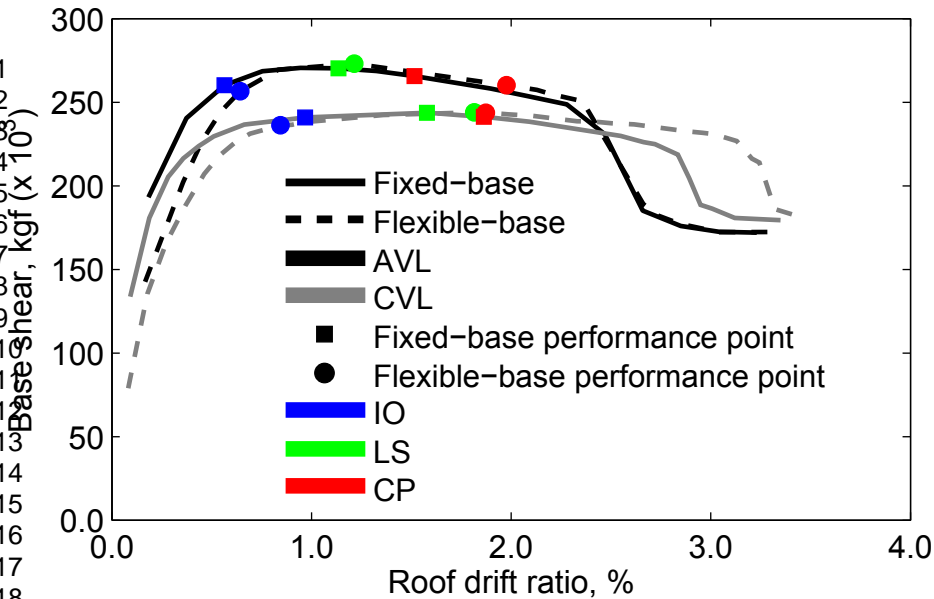
(b)



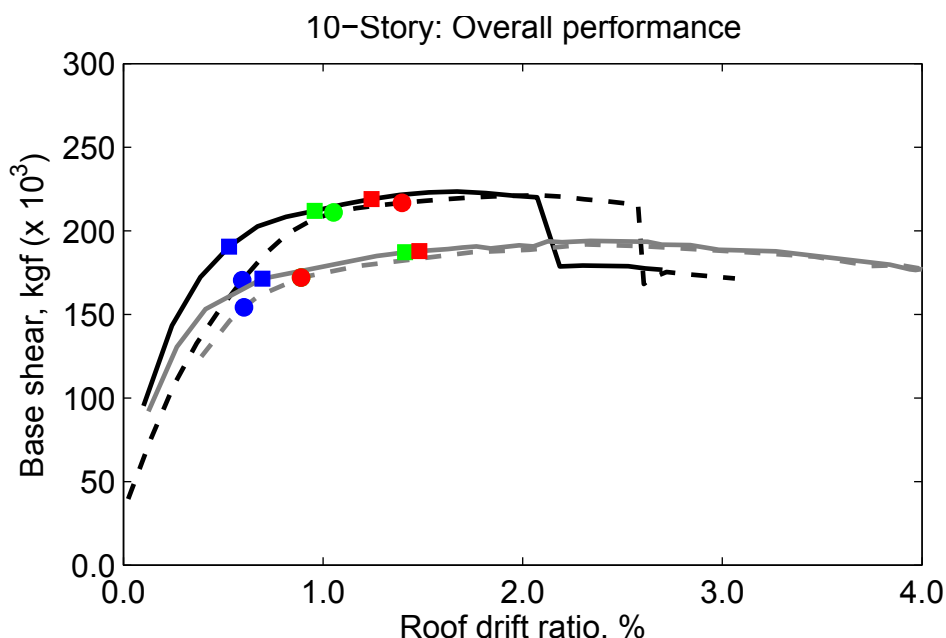
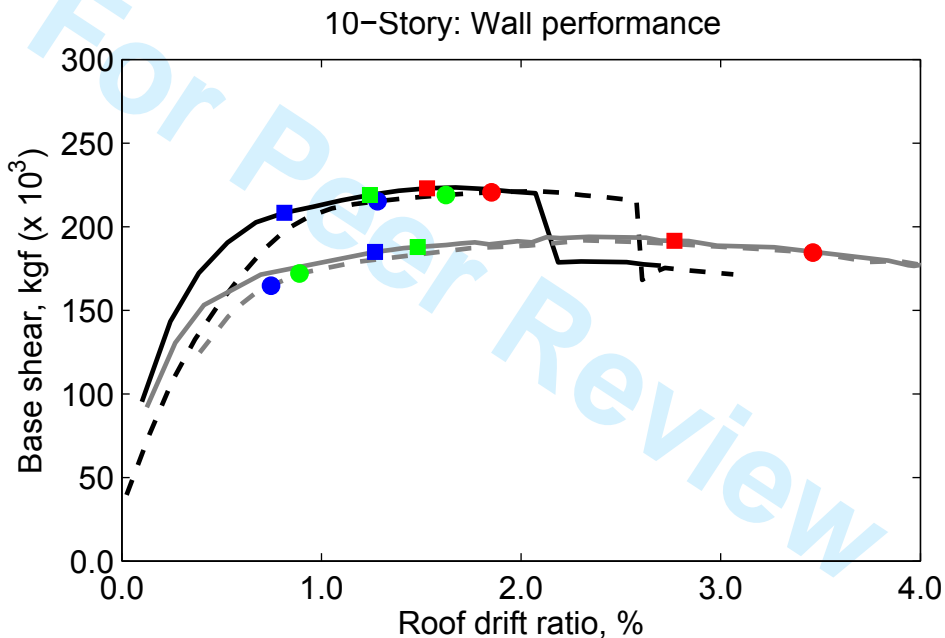
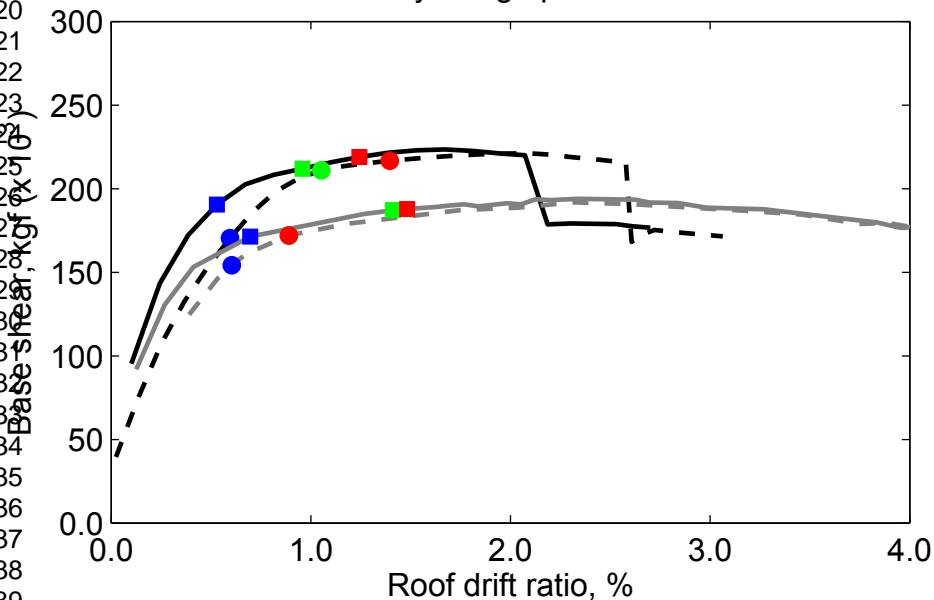


1
2
3
4
5
6
7
8
9
10
11
12
13
14
15
16
17
18
19
20
21
22
23
24
25

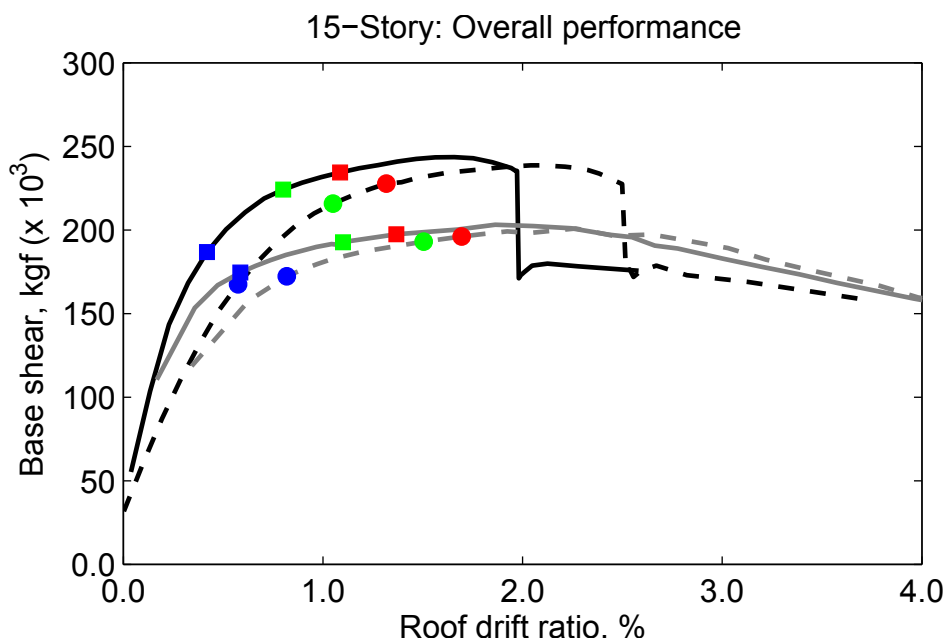
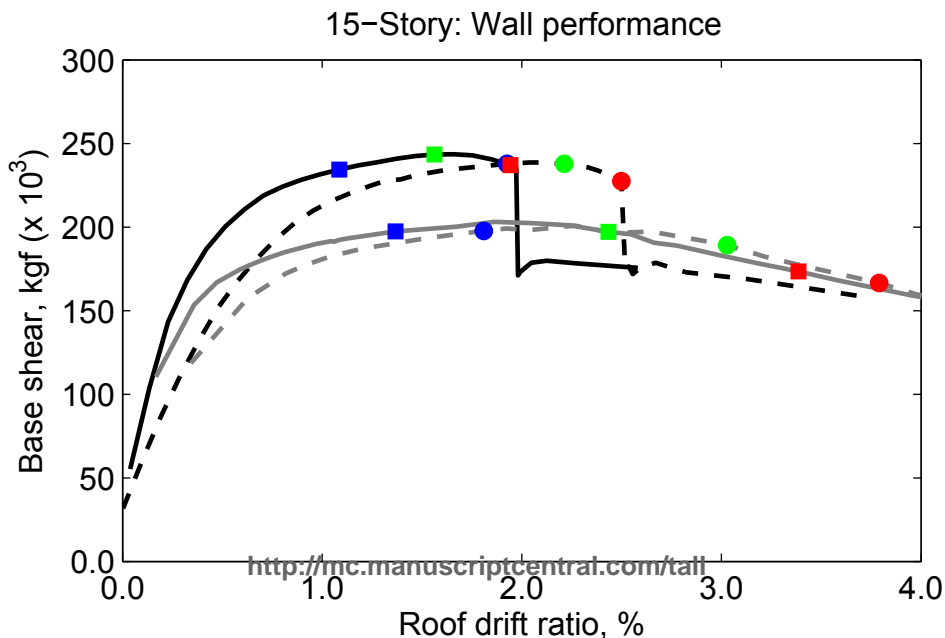
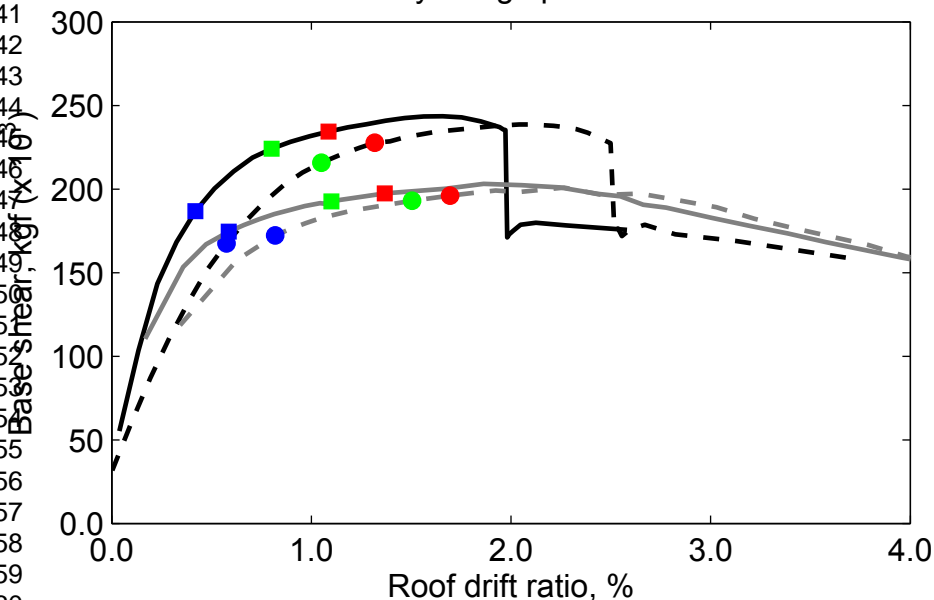
3-Story: Hinge performance



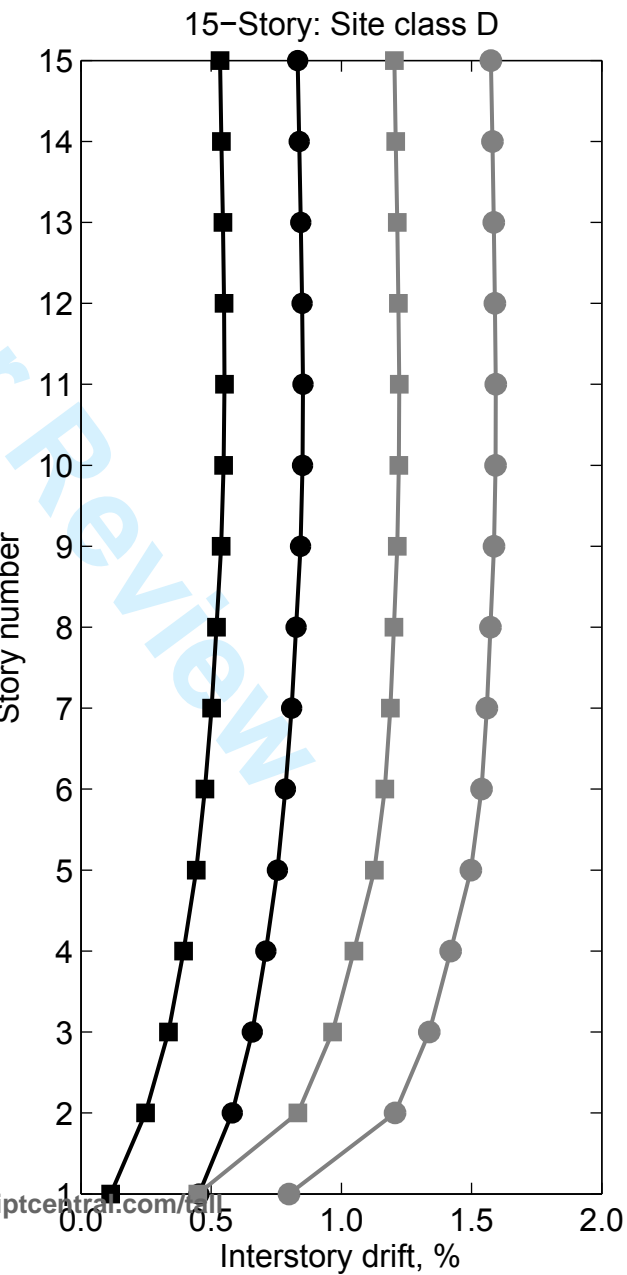
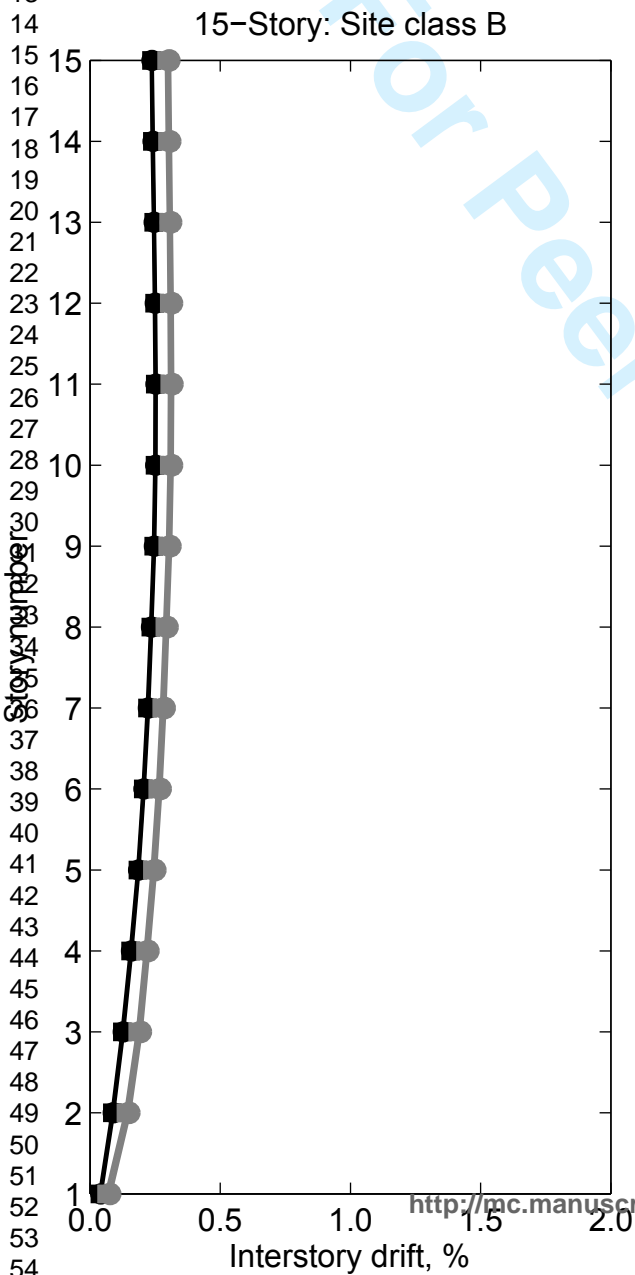
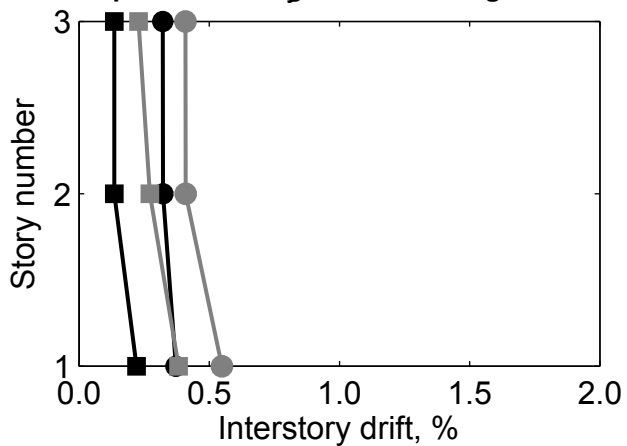
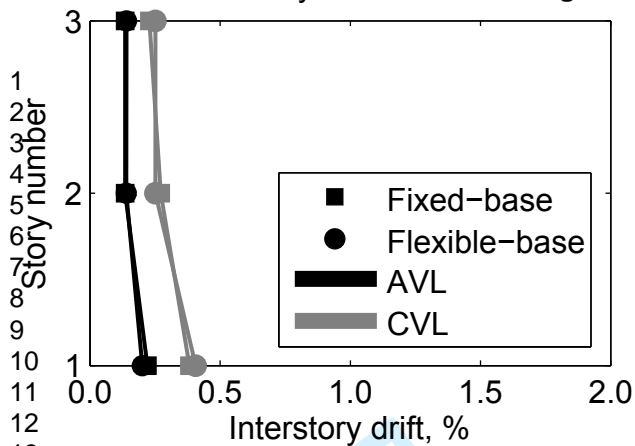
10-Story: Hinge performance



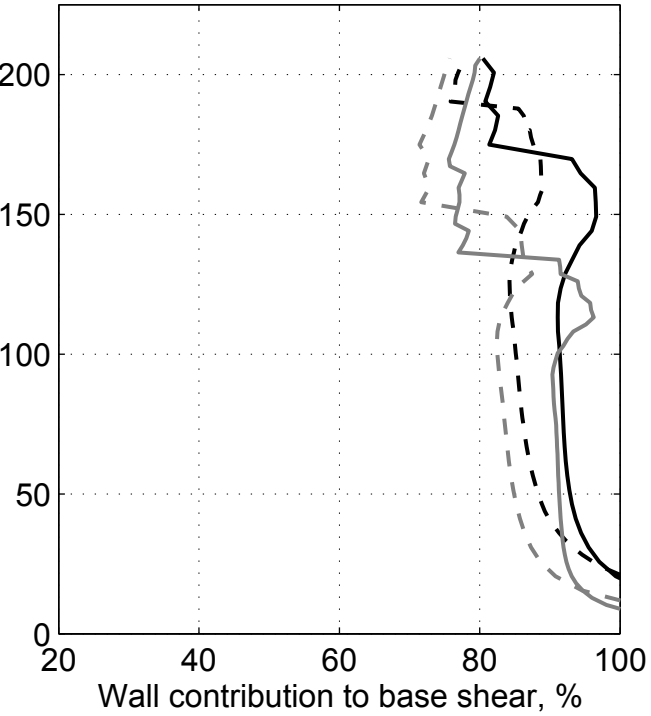
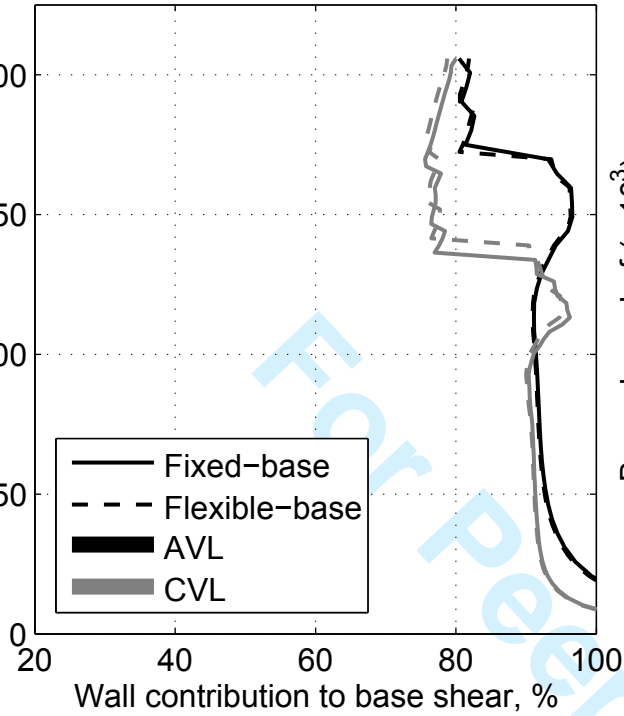
15-Story: Hinge performance



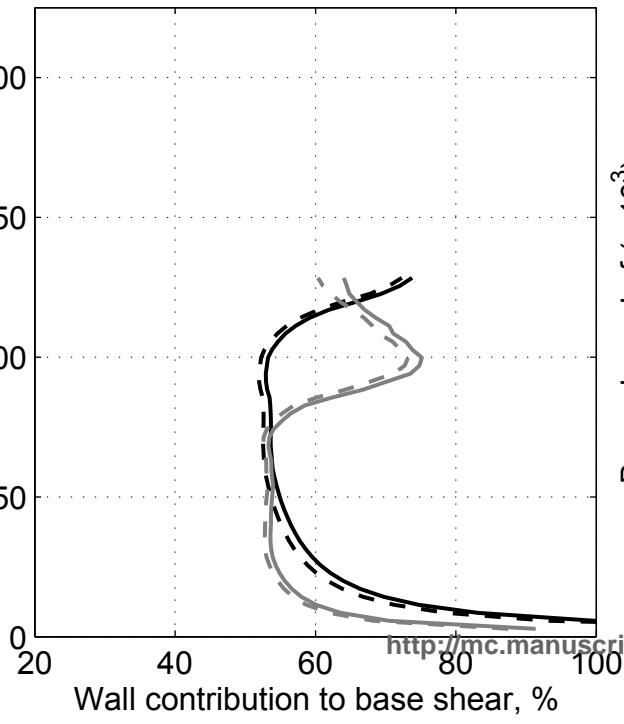
For Peer Review



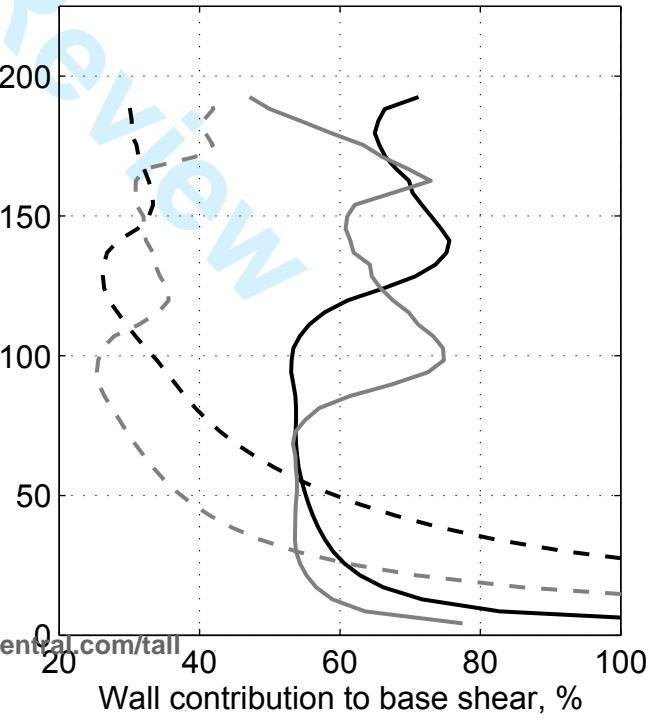
1
2
3
4
5
6
7
8
9
10
11
12
13
14
15
16
17
18
19
20
21
22
23
24
25
26
27
28
29
30
31
32
33
34
35
36
37
38
39
40
41
42
43
44
45
46
47

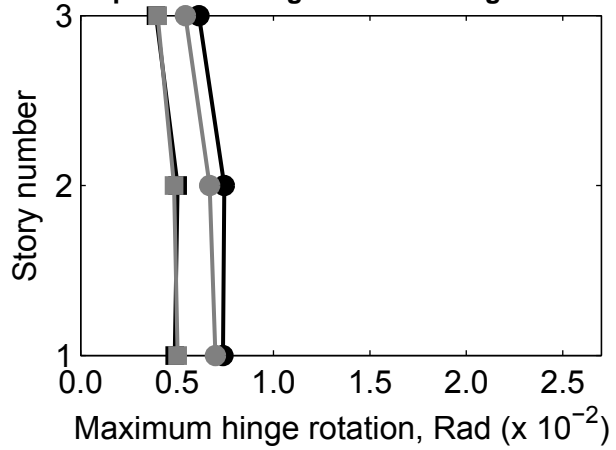
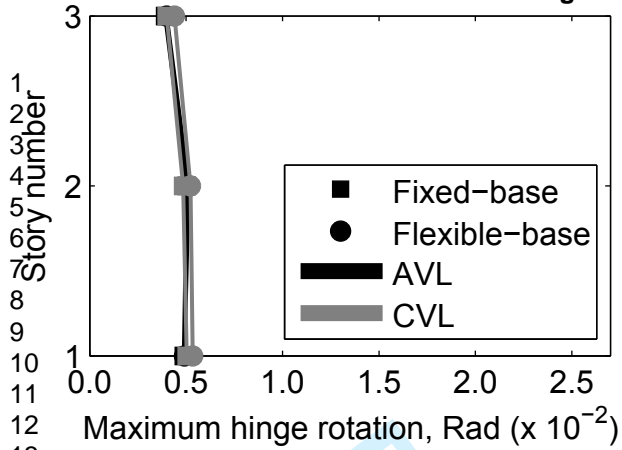


15-Story: Site class B



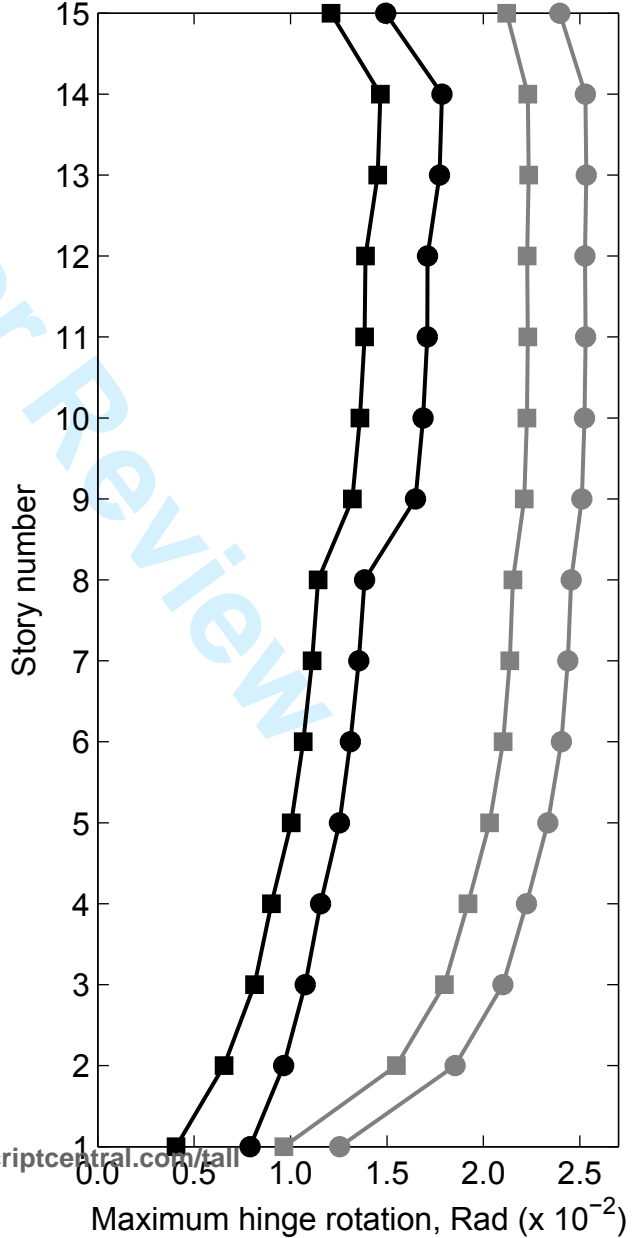
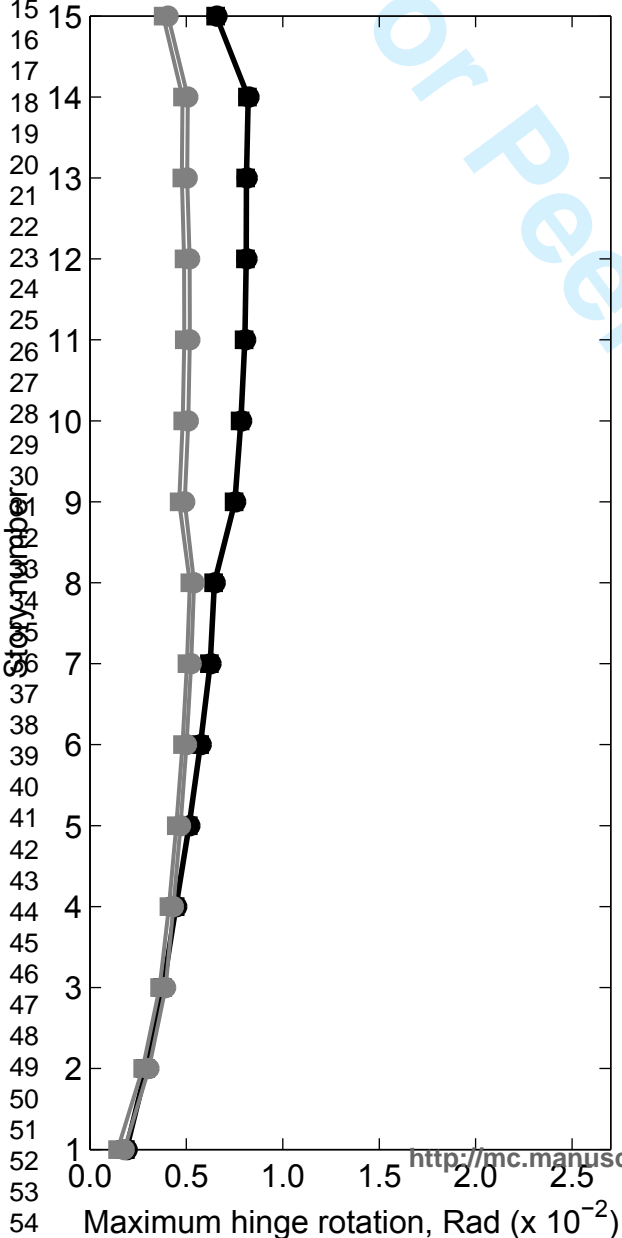
15-Story: Site class D

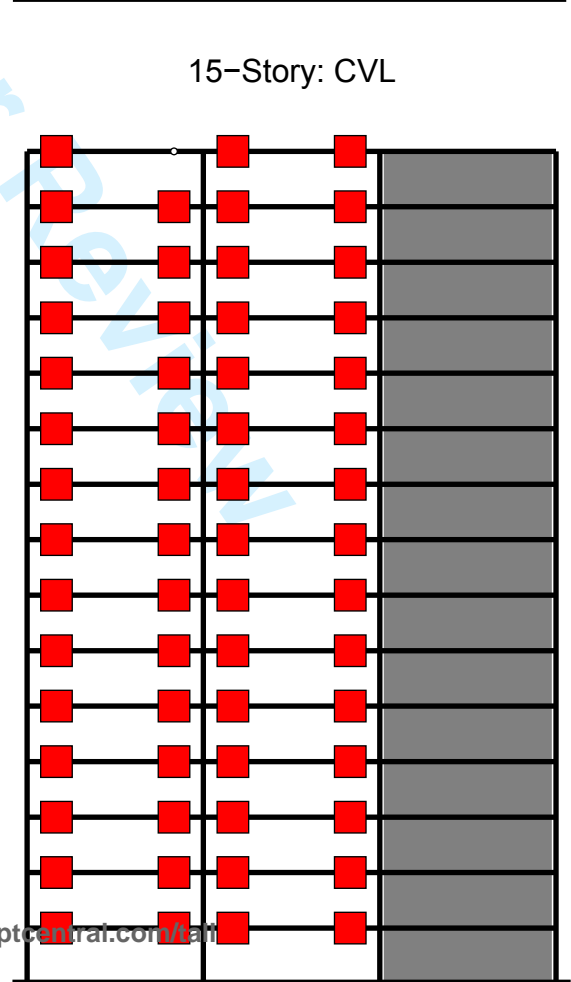
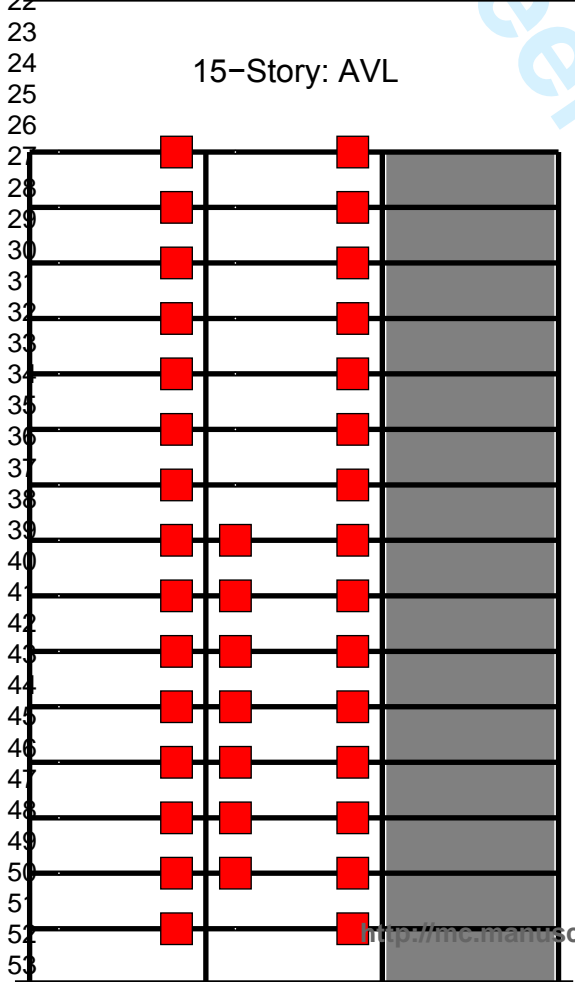
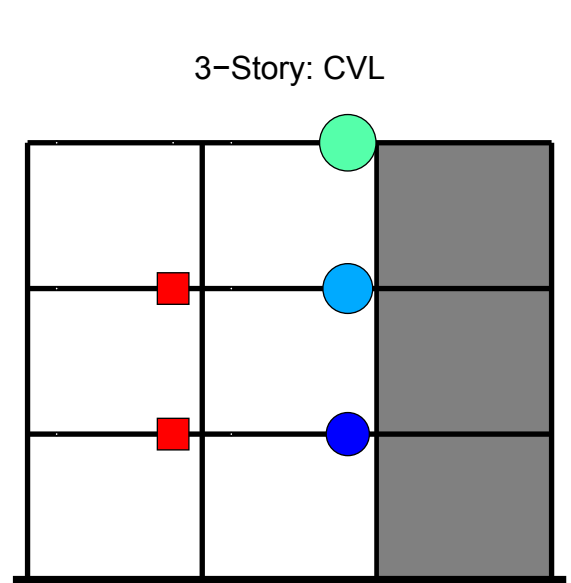
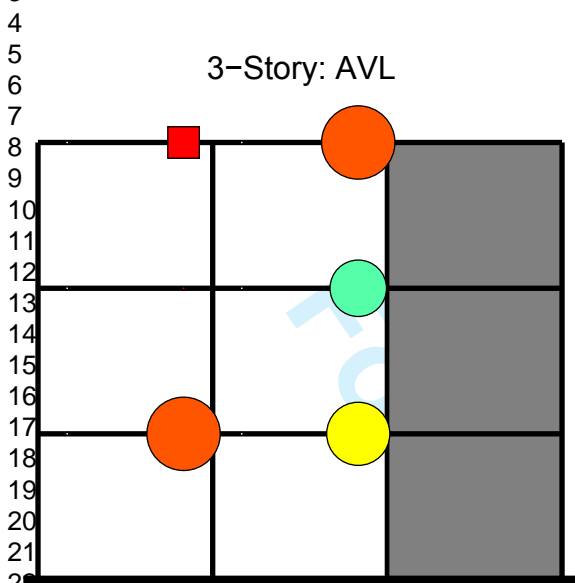




15-Story: Site class B

15-Story: Site class D





Seismic Performance of Reinforced Concrete Shear Wall Frames Considering Soil-Foundation-Structure Interaction

S. Marzban^a, M. Banazadeh^a, A. Azarbakht^{b,*}

^a Department of civil and environmental engineering, Amirkabir University of Technology, Tehran, Iran, 15875-4413

^b Department of civil engineering, Faculty of Engineering, Arak University, Arak, Iran, 38156-8-8349

* Corresponding author: a-azarbakht@araku.ac.ir

Abstract

A practical application of ‘beam on nonlinear Winkler foundation’ approach has been utilized in this paper for a case study on seismic performance of concrete shear wall frames to assess the Soil Foundation Structure Interaction (SFSI) effects. A set of 3, 6, 10 and 15-story concrete shear wall frames located on hypothetically soft, medium and hard soils were designed and modeled using the OpenSees platform. The numerical model of each frame was constructed employing the distributed and lumped plasticity elements as well as the flexure-shear interaction displacement-based beam-column elements incorporating the soil-footing interface. Pushover analysis was performed and the results were studied through two code-based viewpoints: (1) force-based design and (2) performance-based design. A comparison was made afterwards between the frame behaviors in the fixed-/flexible-base conditions. The results indicate some degree of inaccuracy in the fixed-base assumption which is regularly applied in the analysis and design practice. The study emphasizes on how the fixed-based assumption overestimates the design of the wall element and underestimates the design of the connected moment frame.

Keywords: Seismic Performance, Soil-Foundation-Structure Interaction, Reinforced Concrete Shear Wall Frames, Winkler Foundation

1. Introduction

Consideration of the Soil-Structure Interaction (SSI or in its more comprehensive form, Soil-Foundation-Structure Interaction, SFSI), as a phenomenon affecting the dynamic behavior of structures goes back to as early as 1930's [1]. Pioneer studies in this field were limited to the vibrations of machinery foundations and strategic structures such as reactors and oil tanks. However, providing advanced computing tools as well as new insights into the significant effects of SFSI on the behavior of ordinary buildings, today, interaction studies have also found their way in investigation of these structures e.g. [2]. Practically though, one of the interacting substructures (if not both) is overly simplified in interaction studies, depending on whether the structural or the geotechnical aspects of the response are desired. Not to forget that this simplification makes parametric studies reasonable ([3-6] to mention a few). The development of the performance-based earthquake engineering and their increasing application in the design process, the need to roughly incorporate the SFSI effects has become well understood.

Several methods are available for modeling the soil-foundation substructure. They can be roughly categorized into micro and macro modeling approaches. Obviously, micro-element approaches provide the most capabilities when simulating the SFSI. They are still computationally expensive and time-consuming [7]. This turns into a challenging concern when it comes to the uncertainty analysis where a large number of simulations are required. Indeed in this context, rather straightforward modeling methods facilitate the analysis process. Therefore, often in practical SFSI problems, the application of simple methods such as Winkler approach is preferred.

Winkler model, in the simplest form, reduces the soil medium to a finite number of similar discrete and independent linear springs. Many numerical studies have focused on the application of the Winkler method to deal with the SFSI problems. For instance, Psycharis surveyed the dynamic behavior of structures with possibility of uplift in the form of rocking motion [8]. Later on, during two separate studies by Yim and Chopra, response of a single degree of freedom oscillator rested on a two spring-damper system was investigated and the methodology was generalized for a multi-degree of freedom system [9, 10]. In a similar way, Nakaki and Hart employed elastic compressive-only springs and viscous dampers at the base of shear walls to inspect the positive effects of foundation uplift on their seismic response [11]. Recently, Pacific Earthquake Engineering Research Center (PEER) released two reports [12, 13] in 2005 and 2007, with a concentration on the numerical modeling of surface foundations. Both reports attempted to introduce a practical application of the Winkler concept to nonlinear SFSI modeling. The proposed model consisted of vertical nonlinear independent springs, distributed along the foundation length and allowed for uplift, rocking, settlement and radiation damping. Considering its capabilities, the former model was chosen to mainly account for the construction of the ‘beam on nonlinear Winkler foundation’ model in this study.

1.1. Objective of the study

The present study tends to assess the nonlinear behavior of concrete shear wall frames under lateral static load (pushover analysis). It also emphasizes the efficiency of the simple yet sufficiently accurate 'beam on nonlinear Winkler foundation' model. Numerous 2D concrete shear wall frames with different structural and geotechnical features were studied and the results were compared for the fixed-/flexible-base conditions. The comparison was mainly conducted by calculating the well-known and conventional seismic design parameters such as period-based ductility (μ_T), overstrength factor (Ω) and response modification factor (R) as well as the displacement-based performance of the frames.

2. Methodology

Generally, the accuracy of the pushover analysis, when predicting the structural performance, is a matter of controversy. However, this simple method provides a useful understanding of the expected behavior of structures [14]. Therefore, this study was based on the pushover analysis results. Computation of the results according to the nonlinear dynamic analysis is the subject of a future study. To perform the pushover analysis, the lateral forces were applied to a group of selected frames in the form of the recommended patterns of FEMA450 guidelines [15]. The lateral forces distributions are relative to the mass and the height. Later, the pushover curves were calculated based on two methodologies i.e. force-based design and performance-based design.

2.1. Force-based design approach

In the force-based design approach the bilinear ideal pushover curves were constructed and the two seismic design parameters, μ_T and Ω , were determined based on FEMA695 guidelines [16]. Subsequently, the response modification coefficient was calculated. According to FEMA695 guidelines, the ideal bilinear curve was used to characterize the pushover curves, as schematically shown in Figure 1. $\delta_{y,eff}$ and V_{max} designate the effective yield roof drift displacement and the maximum base shear resistance, respectively.

Figure 1 - Idealized nonlinear static pushover curve based on FEMA695 guidelines.

Ω and μ_T were then computed through equations $\Omega = V_{max}/V$ and $\mu_T = \delta_u/\delta_{y,eff}$ as specified in the mentioned guidelines where δ_u corresponds to the ultimate roof displacement. As it is clear, the design base shear (V), corresponding to a point of 'significant yield' in the pushover curve, needs to be identified. Due to the lack of a code definition, the significant yield point needs to be implicitly characterized for concrete shear wall frames. Hence, the occurrence of full yielding in the tensional boundary element of the shear wall was chosen to represent the significant yield point, based on a rational engineering judgment. Evidently, a similar explanation was not applicable to the 3-story frames due to their shear-dominant behavior. Thus concerning the uncertainties inherent in the definition of a significant shear yield in a shear wall element, Ω was not calculated for these frames. With Ω and μ_T being available, the response modification factor was computed according to Equations (1) and (2) in which V_E is the elastic seismic force demand. R_s , R_μ and R_R are the reduction coefficients due to structural over-strength, ductility and redundancy, respectively. It must be noted that R_R was the same for fixed-/flexible-base frames and was set equal to one.

$$R_s = \Omega$$

$$R_\mu = \begin{cases} R_\mu = 1.0 & T \leq 0.03 \text{ s} \\ R_\mu = \sqrt{2\mu_T - 1} & 0.12 \text{ s} \leq T < 0.5 \text{ s} \\ R_\mu = \mu_T & 1.0 \text{ s} \leq T \end{cases} \quad (1)$$

$$R = \frac{V_E}{V_s} = R_s R_\mu R_R \quad (2)$$

2.2. Performance-based approach

In the performance-based approach the performance point was to be found by means of the displacement coefficients

method based on FEMA273 guidelines [17]. In this method, the expected displacement of the structure at the desired performance (so called target displacement) is calculated by modifying the elastic displacement. This is done through applying some coefficients to estimate the nonlinear structural response. *Equivalent displacements* approximation which forms the basis for the displacement coefficients method implies that the method is only applicable to flexible structures. Moreover, the goal of this study was to obtain and compare the performance of fixed-/flexible-base concrete shear wall frames rather than to calculate the target displacement as a part of the design process. Therefore, three performance levels namely the Immediate Occupancy (IO), Life Safety (LS) and Collapse Prevention (CP), were considered in accordance with FEMA356 guidelines [18]. The status of each beam and wall element was checked for the three performance levels according to Tables 6-7 and 6-18/6-19 of the guidelines throughout the pushover analysis. At each step of the analysis if a member failed to fulfill the criteria specified in the code, the loading step was recorded as the step in which the member has reached the desired performance level. Subsequently, it was assumed that a structural system has achieved its performance level if at least one of its members has already met that performance level. Eventually, the performance levels of IO, LS and CP were determined and located on the pushover curves for each frame. Columns were not checked in this regard since the strong-column weak-beam design concept made them less vulnerable to the formation of the plastic hinges before the beams.

3. Numerical modeling

This study attempted to cover a wide range of interaction problems in terms of the superstructure and the soil characteristics. Hence, concrete shear wall frames with 3, 6, 10 and 15 stories and three spans were considered, as shown in Figure 2. The hard, medium and soft soils were, in the same order, introduced through site classes B, C and D based on FEMA450 guidelines. Satisfactory values for the design parameters of the specified site classes were estimated according to several well-known geotechnical references [19-26]. Selected values from the recommended ranges are presented in Table 1. The geotechnical design parameters in this table include E modulus of elasticity, G shear modulus, γ specific weight, D_r relative density and μ poisson's ratio of the soil. It is necessary to note that uncertainties play an important role in the characterization of the soil behavior. However, considering the structural (rather than the geotechnical) aspects of the present study, the provided values of Table 1 could be reasonably accepted for common practice.

Figure 2 - Schematic elevation of the studied frames.

Gravity loads were selected based on values typically employed in engineering practice. Therefore, 3, 6, 10 and 15-story frames had masses equal to 307, 640, 927 and 1511 tons, respectively. Further, equivalent lateral design forces were determined based on FEMA450 guidelines i.e. the design spectrum for each site class was derived and the corresponding design base shears were calculated as presented in Table 2. Both gravity and seismic loads were later imposed on the frames according to the additive and counteractive load combinations of ASCE7-05 standard [27] (the reader is referred to section 12.4.2.3 of ASCE7-05 for further details).

Frames were designed as special frames based on FEMA450 guidelines. According to these guidelines, 15-story frames had to be designed considering dual lateral resisting systems. Thickness of the shear wall was chosen to be 0.25 m in 3/6-story frames and 0.30 m in 10/15-story ones. Strip footings of width 2.0-4.6 m, length 19.6-20.0 m and fixed height 1.0 m, were designed for all frames. Subsequently, the complete numerical models of the concrete shear wall frames were constructed through an appropriate assembly of nonlinear shear wall elements and nonlinear beam-column elements.

3.1. Moment-resisting frame modeling

Beams with concentrated plastic hinges and columns of fiber section were employed to simulate the nonlinear flexural behavior of the moment frames. The *beamWithHinges* element was used to model beams. Hence, a pre-determined length at both ends was allocated to the plastic hinges and an elastic material was assigned to the mid-span. Since the nonlinear behavior was assumed to be focused in the hinges, expansion of the nonlinearity to the elastic region was less likely to happen [28]. Thus, the coefficient of cracking was set equal to 0.5 for the elastic segment of the beams. Nonlinear behavior of the plastic hinges was defined in accordance with Haselton et al. [29]. Essential relationships are proposed in their study based on the calibration of numerous test results in the form of the tri-linear backbone curve suggested by Ibarra [30, 31]. An important feature of the model is that softening due to concrete crushing, reinforcement buckling and yielding and bond slip can be considered in the negative stiffness region, namely post cap behavior [29].

The tri-linear Ibarra model, as discussed above, was employed in the OpenSees [32] platform using the *Clough* material proposed by Altoontash [33]. Subsequently, *Uniaxial* sections with pre-defined $M - \theta$ according to the *Clough* material, were assigned to the plastic hinges. It should be noted that all parameters calculated to form the Ibarra model were in terms of rotations. In order to make them applicable to a *beamWithHinge* element, the simple equation $\phi = \theta/L$ (ϕ curvature, θ rotation and L plastic hinge length), was used to transform rotations into curvatures. This is an advantage of the selected beam

1
2
3 element [34]. The plastic hinge's length was set to be equal to beam's height for all cases.

4 Columns were modeled by means of the fiber section concept with the capability of developing distributed plasticity along
5 the element's length. This choice was made mostly due to the fact that the flexural behavior in columns is highly dependent on
6 the interaction of their axial and bending forces. However, the aforementioned approach for beams was incapable of
7 considering variable axial forces during the analysis. The fiber sections were assigned to *dispBeamColumn* elements. Each
8 element was divided into four sub-elements in a story level to provide more accuracy.

9 10 3.2. Shear wall element modeling

11 Recently, 'Flexure-Shear Interaction Displacement-Based Beam-Column' element has been developed in the OpenSees
12 platform based on the concept of formerly used Multiple Vertical-Line-Element Model (MVLEM). In this new element, the
13 previous multiple vertical columns are defined as fibers of a section. The interaction between the flexural and shear behaviors
14 is provided by incorporating a membrane material model. The flexure-shear interaction displacement-based beam-column
15 element was thus selected to model the shear wall element in OpenSees because of its inclusive features. In particular, with its
16 application, the numerical models showed proper agreement with the characteristics of the designed concrete shear wall
17 frames. More information about the element can be found in Orakcal et al. [35].

18 Definition of the boundary elements was also provided in the model. Hence, the resulting shear wall element would take the
19 form of a single column. Although, attaching this column to the moment frame was quite problematic. To cope with this
20 problem, the mid-panel of the shear wall was constructed with the flexure-shear interaction displacement-based beam-column
21 element while the boundary elements were modeled as columns of the main frame. To enhance the accuracy, each element was
22 divided into four sub-elements in a story level. End nodes located on the same elevation of the boundary elements and the mid-
23 panel column element were then joined by means of rigid beams. This provided an integrated simulation of the whole shear
24 wall system. As it is obvious, the system could benefit from the top features of both flexure-shear interaction model and fiber
25 section.

26 27 3.3. Soil-footing interface modeling

28 The beam on nonlinear Winkler foundation was employed to model the soil-footing interface. It captures both geometrical
29 (uplift and rocking motions) and material (nonlinear behavior of the soil) nonlinearities. Furthermore, it allows for likely
30 changes in soil springs' stiffness and spacing along the foundation length. In this study, the numerical model based on the
31 beam on nonlinear Winkler foundation was constructed through assigning *dispBeamColumn* and *zeroLength* elements to the
32 strip footing and soil springs, respectively. It is worth mentioning that the beam at the base of the shear wall was set to be rigid
33 due to high flexural stiffness that the shear wall added to the footing's rigidity. In addition, the footing was constrained against
34 sliding [13, 36 and 37]. In order to define the Winkler springs, first their properties were determined according to different site
35 classes and the corresponding footing dimensions. Second, *Qzsimple1* material (in Opensees) was chosen to represent the soil
36 behavior based on the computed parameters. The Gazetas concentrated stiffness [38] was employed to define the stiffness of
37 the soil springs. Hence, the total vertical and rotational stiffness of the footing-soil systems were found according to Gazetas
38 proposed relations as shown in Table 3. A specific distribution of the Winkler springs with varying stiffness was later selected
39 for each system to produce the same total vertical and rotational concentrated stiffness.

40 It has been experimentally established that during the rocking motion, a higher stiffness would develop in the soil medium at
41 the compression zones. The so-called rounding phenomenon happens to retain the stability of the structure [12]. Accordingly,
42 more stiff springs were placed at the ends of the footing strip to supply the rotational stiffness of the soil-footing system. The
43 end lengths were determined based on [12]. Finally, a configuration of vertical springs of particular stiffness, located in the
44 middle and end zones of the footing strip, was chosen based on [12] to result in the total rotational stiffness. The strength of the
45 Winkler springs was calculated based on the bearing capacity of the foundations. Among several equations available to
46 determine the bearing capacity, Terzaghi's relationship (1943) is widely employed in engineering problems [19]. However, a
47 more rigorous form of the Terzaghi's relationship, proposed by Meyerhof (1963) [19], was selected to estimate the foundation
48 bearing capacities in this study as presented in Table 4. The final numerical model of the studied systems is schematically
49 shown in Figure 3.

50
51
52 Figure 3 – Numerical model of the studied concrete shear wall frames.

53 4. Nonlinear static analysis results

54 Before the lateral load was applied, the Additive and Counteractive Vertical Loadings (AVL and CVL) were separately
55 imposed on the frames according to the load combinations discussed in section 3. In addition, settlements due to the gravity
56 loads were considered for the flexible-base models. Thus, in these cases, the pushover analysis was performed on the frames
57 settled due to the gravity loads. Figure 4 shows the corresponding gravity settlements for 3/15-story frames along the footing
58 length.
59
60

Figure 4 – Settlements due to gravity for 3/15-story frames founded on site classes B, C and D.

4.1. Fundamental period elongation

The fundamental period shifted significantly, as seen in Figure 5, due to the contribution of the rocking motion in the first mode. This was particularly evident in lower height frames founded on softer soils. The observed increase tended to disappear as the soil got stiffer and/or the frame got more flexible. Furthermore, site class was less effective on the period elongation of high-rise frames.

Figure 5 - The fixed and flexible-base fundamental periods of the studied frames.

4.2. Study of pushover curves based on force-based design codes

After computing the required parameters, V_{max} , C_0 and $\delta_{y,eff}$, the approximate bi-linear pushover curves were calculated according to FEMA695 guidelines, as seen in Figure 6 for 3/15-story frames. The SFSI significantly decreased the initial stiffness of all frames. This substantiated the fundamental period elongation. However, higher (i.e. more flexible) frames were less affected in this regard. Also it is noteworthy to mention that the total seismic capacity (V_{max}) remained approximately the same when transforming from fixed to flexible-base condition. Namely, the SFSI did not alter the total base shear capacity but rather made it occur at larger overall displacements.

Further, the influence of the gravity loads on the SFSI was examined. Footing uplift was assumed to be more likely when the structure was under low gravity loads. Here, it was found that the low-rise frames (3/6-story) under CVL were more affected by the SFSI than those frames under AVL. This trend, however, got reversed for high-rise frames (10/15-story), i.e. SFSI affected frames with AVL more than those with CVL. In the former frames, low gravity loads tended to undermine the overall stability of the structural system and thus resulted in less effectiveness of the SFSI in contradiction to low-rise frames.

Figure 6 - Base shear vs. roof drift ratio curve and its bilinear idealization for 3/15-story frames founded on site classes B and D.

Following that δ_u was determined based on FEMA695 guidelines, the period-based ductility, μ_T was calculated. Figure 7(a) demonstrates the values of μ_T in terms of the site class and the frame height. It was clearly recognized that the SFSI substantially reduced μ_T . Also, relatively large differences were observed between the ductilities on rigid (B) and non-rigid (C and D) soils. Accordingly, the rigid base assumption for frames founded on non-rigid soils could lead to a misestimating of the μ_T . Moreover, as it was expected, the descending inclination flattened when frames moved toward more flexibility. Next, having V_{max} and V_s in hand, the overstrength coefficient was calculated. As discussed previously, the overstrength coefficient was not computed for 3-story frames because of their shear-dominant behavior. Hence, Figure 7(b) shows the values of Ω for 6, 10 and 15-story frames. It was clear that changes in Ω due to SFSI were not much of concern.

Ductility and overstrength coefficients, were later employed to determine R_u and R . R_u was calculated using Newmark and Hall relationships [39] (Equation (1)) as illustrated in Figure 8. Although, in the case of 6-story frames Equation (1) offered different formula for R_u since the fundamental period of these frames fell in the transition area between the constant acceleration and velocity regions of the response spectra. To avoid this discontinuity, the equation proposed by Krawinkler and Nassar [39] was used for 6-story frames. Subsequently, the reduction factor was determined according to Equation (2) as it is shown in Figure 8. It could be observed that R decreased noticeably in frames with SFSI when compared to the fixed-base frames. When investigating the effect of the site classes, R followed a clear downward trend from hard to soft soils. Again, large differences were seen between the reduction factor on rigid and non-rigid soils. Namely, the rigid base assumption might not result in true values for R in the case of frames founded on non-rigid soils. Generally, special attention should be paid to the design of flexible-base frames because along with the period elongation, they paradoxically show a decrease in their reduction factor R .

Figure 7 - The normalized (a) period-based ductility (b) overstrength coefficient.

Figure 8 - The normalized (a) reduction factor due to ductility (b) reduction factor.

4.3. Study of pushover curves based on performance-based design codes

Performance levels were obtained based on the status of the beams plastic hinges and the wall elements. IO, LS and CP performance levels were determined for each of the aforementioned members according to FEMA356 guidelines. The mentioned performance levels were detected for wall and beam elements individually. Subsequently, the performance points of the global frame-wall systems were estimated as discussed before. Selected results are shown in Figure 9 for frames located on the site class D.

According to Figure 9, the seismic performance was generally improved in the flexible-base condition. As expected, improvements were extended when soil stiffness decreased from the site class B to the site class D. This was not the case for 10-story frame under CVL. It should be noted that based on FEMA450 guidelines, 10-story frames are not required to be designed as dual lateral resisting systems. Hence, these frames were designed as special RC shear wall frames (which implies that the moment frames were solely designed to withstand gravity loads) with the intention to check the adequacy of the code-specified design in the presence of SFSI. It was however obvious from the results that in the flexible-base condition, the moment frames contributed more to the lateral resisting of the systems when compared to the fixed-base condition. This was specifically true for the higher frames. Consequently, in the case of flexible-base 10-story frame, the moment frame was loaded beyond its design forces and deformations. Therefore, it failed to provide a reasonable behavior and plastic hinges were formed at lower loading steps. Nevertheless, 10-story frame under AVL did not follow the same trend owing to its more stability under larger gravity loads and thus, less tendency to deform.

Performance of the walls was also improved in the flexible-base cases. Namely, a certain performance level was attained under the application of a larger force in the flexible-base state when compared to the fixed-base condition. As it was expected the trend was not the case for flexible-based 10-story frames as a result of the weak performance of the connected moment frames. Finally, it was difficult to find a general trend for the performance of the beams plastic hinges. Nonetheless, for low-rise frames the SFSI tended to weaken the performance. For 15-story frames, however, a certain performance level was achieved at a larger displacement when SFSI was considered. The particular case of 10-story frames is formerly discussed.

Figure 9 - Plastic hinges, shear wall element and the overall performance of 3/10/15-story frames founded on site class D.

4.4. Comparison of the nonlinear static behavior of the frames in the fixed and flexible-base conditions

Push-over curves were further studied in order to assess the nonlinear static behavior of the frames and their individual members, from both qualitative and quantitative aspects. Each frame was pushed to a base shear equal to 80% of its total base shear capacity (V_{max}) through a force-controlled loading. Most deviations in the pushover curves of the flexible and fixed-base states were observed prior to the mentioned base shear. A unique lateral force limit was chosen for identical frames under different gravity loadings in order to make more sensible comparisons. Table 5 contains the mean values of the applied lateral forces normalized to the corresponding design base shears. Nonlinear static behavior of the fixed and flexible-base frames was examined as presented in the following sections.

4.4.1. Comparison of the overall behavior

Study of the story drifts provides an overview of the absorbed seismic energy in the form of the strain energy. Generally, in the flexible-base condition, the footing uplift led to a rigid body motion of the stiff superstructure which essentially contributed to the overall displacement. Figure 10 shows the relative story displacements for 3/15-story frames. The story drifts decreased in the flexible-base cases as seen in Figure 10. Further, AVL and CVL presented different contributions to the relative story displacements. In 3/6-story flexible-base frames, CVL appeared to increase uplift and subsequently, decrease the interstory drift. In the 10/15-story frames under CVL, however, the SFSI was less influential on the interstory drift.

4.4.2. Comparison of the shear wall behavior

The resisting base shear was primarily developed in the mid-panel of the shear wall. Therefore, the contribution of the wall element to the base shear was investigated by calculating the ratio of the base shear in the mid-panel to the total base shear. This is presented in Figure 11 for 3/15-story frames. According to the figure, the mid-panel shear was substantially reduced when considering the SFSI effects. In addition, for flexible-base low-rise frames the participation curve was shifted upward along the vertical axis when compared to the fixed-base condition. In other words, a specific percent of contribution was achieved at larger lateral forces in the flexible-base state. In high-rise frames the wall contribution showed more reduction in comparison to the low-rise frames. However the SFSI was still more effective on stiffer frames. In high-rise frames the overall participation of the shear wall in the lateral resisting base shear was less than that of the low-rise frames. Therefore the reduction came across as being larger in percentage for the smaller values. It is worth noting that the axial forces in the shear wall boundary elements were also controlled. The results showed that the axial forces were not largely affected by the SFSI.

Figure 10 - Distribution of the interstory drift for 3/15-story frames.

Figure 11 – Wall contribution to the base shear for 3/15-story frames.

4.4.3. Comparison of the moment frame behavior

The interaction of the shear wall element and the connected moment frame became more crucial when the interaction of the whole system with the soil-footing interface was introduced to the problem. In order to achieve a quantitative perception of the moment frame performance, the beams plastic hinges were checked in the flexible-base state and compared to those in the fixed-base condition. The distribution of the beams maximum rotations is shown in Figure 12 along the frames height. It was obvious that beams had experienced more rotations at their ends in the presence of SFSI. Note that in the low-rise frames, the increase was more than that of the high-rise ones. Moreover, in all cases, a decrease in the soil stiffness intensified the increase in the beams rotations. In particular, for 3-story frame founded on site class D the increase was as much as 50% whereas the corresponding value for the 15-story frame hardly reached 15%.

The beams plastic rotations in the flexible-base state were also computed and compared to the corresponding fixed-base values. They are presented schematically in Figure 13 for 3/15-story frames. The presented values were obtained by normalizing the hinge plastic rotation difference between the fixed and flexible-base conditions to that of the fixed-base condition. It was apparent that the SFSI effects increased the demand on the beams and subsequently the moment frame. In the case of 3-story frames, the increase percentage ranged from negligible for site class B to considerable (more than 100%) for site class D. In the high rise frames, the behavior of the beam hinges mainly altered from elastic in the fixed-base state to inelastic in the flexible-base condition. In other words, in contrast to the flexible-base state, no plastic rotation occurred in the fixed-base condition.

Figure 12 - Distribution of the maximum beams rotations for 3/15-story frames.

Figure 13 - Distribution of the plastic rotations for 3/15-story frames.

5. Conclusions

The seismic performance of a selected number of concrete shear wall frames was assessed through the static nonlinear analysis by taking the SFSI into account. A range of soft to hard soils was modeled by means of the Winkler foundation method. In the first step, a force-based code approach was employed to study the SFSI effects on the evaluation of the seismic design parameters. When compared to the fixed-base condition, the reduction factor, R adopted a descending trend from hard to soft soils for all the flexible-base frames whereas the fundamental period followed an ascending trend in the same context. Hence, careful attention should be paid to the newly introduced design conditions in which the reduced reduction factor and increased fundamental period inversely impact on the estimated design lateral force. This is of great importance in the force-based design approach, since it is established on the concept of reducing the elastic design force in order to take the nonlinear structural behavior into account.

In the second step, the seismic performance of concrete shear wall frames was studied. The overall seismic performance of the frames was enhanced in all the studied cases except for the 10-story frames under CVL. The moment resisting frame failed to efficiently involve in providing the lateral resistance, in the case of 10-story frames, mostly because it was designed to withstand gravity loads according to FEMA450 guidelines. Consequently, the shear wall element and the beam plastic hinges presented weak performance in 10-story frames. The shear wall performance was enhanced in all other cases. Yet, the plastic hinges did not follow a noticeable trend. For the most part, the SFSI improved the plastic hinges performance in the high-rise frames in contrast to the low-rise ones.

Eventually, the seismic behavior of concrete shear wall frames was studied and compared in the fixed/flexible-base conditions. The results revealed that the interstory drifts and the panel shear in the shear walls were reduced in the flexible-base condition. However, these effects tended to fade when the numbers of stories were increased. Further, the beam end rotations were intensified under the impacts of the SFSI especially in the case of stiffer frames founded on softer soils. In the final analysis, it should be noted that the SFSI consequences on the seismic performance of concrete shear wall frames account for far more complex considerations than the period elongation alone. In fact the use of the fixed-base assumption may lead to bias in evaluation of the real structural forces and displacements.

References

- [1] Allotey, N. K. (2006). *Nonlinear soil-structure interaction in performance-based design*. (PhD thesis). University of Western Ontario, London, Canada.
- [2] Bárcena, A., & Esteve, L. (2007). Influence of dynamic soil-structure interaction on the nonlinear response and seismic reliability of multistorey systems. *Earthquake Engineering and Structural Dynamics*, 36(3), S. 327-346.
- [3] Raychowdhury, P. (2011). Seismic response of low-rise steel moment-resisting frame (SMRF) buildings incorporating nonlinear soil-structure interaction (SSI). *Engineering Structures*, 33(3), S. 958-967.
- [4] Avilés, J., & Pérez-Rocha, L. E. (2005). Influence of foundation flexibility on R_{μ} and C_{μ} factors. *Structural Engineering*, 131(2), S. 221-230.
- [5] Ghannad, M., & Jahankhah, H. (2007). Site-dependent strength reduction factors for soil-structure systems. *Soil Dynamics and Earthquake Engineering*, 27(2), S. 99-110.
- [6] Avilés, J., & Pérez-Rocha, L. (2011). Use of global ductility for design of structure-foundation systems. *Soil Dynamics and Earthquake Engineering*, 31(7), S. 1018-1026.
- [7] Allotey, N., & El Naggar, M. H. (2008). An investigation into the Winkler modeling of the cyclic response of rigid footings. *Soil dynamics & earthquake engineering*, 28 (1), 44-57.
- [8] Psycharis, I. N. (1982). *Dynamic behavior of rocking structures allowed to uplift*. (PhD thesis). California Institute of Technology, Pasadena, California.
- [9] Chopra, A. K., & Yim, S. C. (1985). Simplified earthquake analysis of structures with foundation uplift. *Structural engineering*, 111 (4), 906-930.
- [10] Yim, S. C., & Chopra, A. K. (1985). Simplified earthquake analysis of multistory structures with foundation uplift. *Structural engineering*, 111 (12), 2708-2731.
- [11] Nakaki, D. K., & Hart, G. C. (1987). Uplifting response of structures subjected to earthquake motions. US- Japan coordinated program for masonry building research. Ewing, Kariotis: Englekirk and Hart.
- [12] Harden, C., Hutchinson, T. C., Martin, G. R., & Kutter, B. L. (2005). Numerical modeling of the nonlinear cyclic response of shallow foundations. Report No. PEER-2005/04. Berkeley: Pacific Earthquake Engineering Research Center, University of California.
- [13] Gajan, S., Hutchinson, T. C., Kutter, B. L., Raychowdhury, P., Ugalde, J. A., & Stewart, J. P. (2007). Numerical models for analysis and performance-based design of shallow foundations subjected to seismic loading. Report No. PEER-2007/04. Berkeley: Pacific Earthquake Engineering Research Center, University of California.
- [14] Vamvatsikos, D., & Fragiadakis, M. (2009). Incremental dynamic analysis for estimating seismic performance sensitivity and uncertainty. *Earthquake engineering & structural dynamics*, 39 (2), 141-163.
- [15] FEMA, (2004). NEHRP Recommended provisions for seismic regulations for new buildings and other structures, FEMA 450-1/2003 Edition, Part 1: Provisions, Federal Emergency Management Agency, Washington, D.C.
- [16] FEMA, (2009). *Quantification of building seismic performance factors*, FEMA P695/2009 Edition, Federal Emergency Management Agency, Washington, D.C.
- [17] Building Seismic Safety Council (BSSC, 1997a). *FEMA 273/274 - NEHRP Guidelines for the seismic rehabilitation of buildings*, Vol. I – Guidelines, Vol. II – Commentary, Washington, DC.
- [18] FEMA, (2000). *Prestandard and commentary for seismic rehabilitation of buildings*, FEMA 356, Prepared by the American Society of Civil Engineers for the Federal Emergency Management Agency, Washington, D.C.
- [19] Bowles, J. E. (1997). *Foundation analysis and design* (5th ed.). London: McGraw-Hill.
- [20] Day, R. W. (2002). *Geotechnical earthquake engineering handbook*. McGraw-Hill.
- [21] Day, R. W. (2006). *Foundation engineering handbook: design and construction with the 2006 international building code*. McGraw-Hill.
- [22] Bell, F. G. (2000). *Engineering properties of soils and rocks* (4th ed.). Wiley-Blackwell.
- [23] Hunt, R. E. (2005). *Geotechnical engineering investigation handbook* (2nd ed.). CRC Press.
- [24] Das, B. M. (2006). *Principles of geotechnical engineering* (6th ed.). Thomson.
- [25] Brown, R. W. (2001). *Practical foundation engineering handbook* (2nd ed.). McGraw-Hill.
- [26] Murthy, V. N. (2003). *Geotechnical engineering: principles and practices of soil mechanics and foundation engineering*. CRC Press.
- [27] American Society of Civil Engineers, (2005). *Minimum design loads for buildings and other structures*, ASCE/SEI 7-05.
- [28] Lowes, L. N., Mitra, N., and Altoontash, A. (2004). *A beam-column joint model for simulating the earthquake response of reinforced concrete frames*. Report No. PEER-2003/10. Berkeley: Pacific Earthquake Engineering Research Center, University of California.
- [29] Haselton, C. B., S. Taylor Lange, A. B. Liel, and G. G. Deierlein (2007). *Beam-column element model calibrated for predicting flexural response leading to global collapse of RC frame buildings*, Report No. PEER-2007/03. Berkeley: Pacific Engineering Research Center, University of California.
- [30] Ibarra, L. (2003). *Global collapse of frame structures under seismic excitations*. (PhD thesis). Department of CEE, Stanford University, USA.
- [31] Ibarra, L. F., Medina, R. A., & Krawinkler, H. (2005). Hysteretic models that incorporate strength and stiffness deterioration. *Earthquake engineering & structural dynamics*, 34 (12), 1489-1511.
- [32] McKenna, F., Fenves, G. L., & Scott, M. H. (2000). Open System for Earthquake Engineering Simulation (OpenSees). University of California, Berkeley.
- [33] Altoontash, A. (2004). *Simulation and damage models for performance assessment of reinforced concrete beam-column joints*. (PhD thesis). Department of Civil and Environmental Engineering, Stanford University.
- [34] Scott, M. H., & Fenves, G. L. (2006). Plastic hinge integration methods for force-based beam-column elements. *Structural Engineering*, 132 (2), 244-252
- [35] Orakcal, K., Massone, L., Wallace, J. (2006). *Analytical modeling of reinforced concrete walls for predicting flexural and coupled-shear-flexural response*. Report No. PEER-2006/07. Berkeley: Pacific Earthquake Engineering Research Center, University of California.
- [36] Beucke, K., Werkle, H., & Waas, G. (1983). Nonlinear soil-structure-interaction with base mat uplift. *7th international conference on structural mechanics in reactor technology*. Chicago.
- [37] Xu, C. J., & Spyarakos, C. C. (1996). Seismic analysis of towers including foundation uplift. *Engineering structures*, 18 (4), 271-278.
- [38] Gazetas, G. (1991). Foundation Vibrations. In H. Y. Fang (Ed.), *Foundation engineering handbook* (pp. 553-593). New York: Van Nostrand Reinhold.
- [39] Miranda, E., & Bertero, V. (1994). Evaluation of strength reduction factors for earthquake resistant design. *Earthquake Spectra*, 10 (2), 357-379.

Table 1 - Selected characteristics for site classes B, C and D.

Soil Type	E (MPa)	G (MPa)	γ (kN/m ³)	D_r (%)	μ
Rock	15000	6000	24	-	0.25
Gravel	200	74.1	21	85	0.35
Sand	65	24	19	75	0.35

For Peer Review

1
2
3
4
5
6
7
8
9
10
11
12
13
14
15
16
17
18
19
20
21
22
23
24
25
26
27
28
29
30
31
32
33
34
35
36
37
38
39
40
41
42
43
44
45
46
47
48
49
50
51
52
53
54
55
56
57
58
59
60

Table 2 - Calculated design base shears (in ton-force).

Lateral Resisting System	Number of Stories	Site Class		
		B	C	D
	10	71.4	89.0	101.0
Shear Wall Frame	6	99.2	106.9	106.9
	3	51.3	51.3	51.3
Dual System (Shear Wall + Moment Resisting Frame)	15	56.8	73.9	85.2

For Peer Review

Table 3 - The soil-footing elastic vertical/rotational Gazetas stiffnesses.

	Site class	Number of stories			
		3	6	10	15
Vertical stiffness intensity	B	5419	3708	2882	2574
K_z/A (MN/m^3)	C	77	53	41	37
	D	25	17	13	12
Rotational stiffness intensity	B	7697	6545	5744	5432
K_{θ_y}/I_y ($MN.m/m^4$)	C	110	93	82	77
	D	36	30	27	25

For Peer Review

1
2
3
4
5
6
7
8
9
10
11
12
13
14
15
16
17
18
19
20
21
22
23
24
25
26
27
28
29
30
31
32
33
34
35
36
37
38
39
40
41
42
43
44
45
46
47
48
49
50
51
52
53
54
55
56
57
58
59
60

Table 4 - Foundation bearing capacity based on Meyerhof's relationship.

	Site class	Number of stories			
		3	6	10	15
Foundation bearing capacity	B	49304	61931	75183	83381
	C	14526	17629	20967	22989
q_{ult} (kPa)	D	5291	6227	7267	7886

For Peer Review

1
2
3
4
5
6
7
8
9
10
11
12
13
14
15
16
17
18
19
20
21
22
23
24
25
26
27
28
29
30
31
32
33
34
35
36
37
38
39
40
41
42
43
44
45
46
47
48
49
50
51
52
53
54
55
56
57
58
59
60

Table 5 - Ratio of the applied lateral force to the design base shear

Umber of Stories	3	6	10	15
Mean Value of the ratio $0.8V_{\max}/V$	4.0	1.9	1.85	2.25

For Peer Review